

**GREEN SYNTHESIS, CHARACTERIZATION OF
COPPER(II) OXIDE NANOPARTICLES AND THEIR
PHOTOCATALYTIC ACTIVITY**

LEONG MEI KEI

BACHELOR OF SCIENCE (HONS) CHEMISTRY

FACULTY OF SCIENCE

UNIVERSITI TUNKU ABDUL RAHMAN

MAY 2016

**GREEN SYNTHESIS, CHARACTERIZATION OF COPPER(II) OXIDE
AND THEIR PHOTOCATALYTIC ACTIVITY**

By

LEONG MEI KEI

A project report submitted to the Department of Chemical Science

Faculty of Science

Universiti Tunku Abdul Rahman

in partial fulfilment of the requirements for the degree of

Bachelor of Science (Hons) Chemistry

May 2016

ABSTRACT

GREEN SYNTHESIS, CHARACTERIZATION OF COPPER(II) OXIDE NANOPARTICLES AND THEIR PHOTOCATALYTIC ACTIVITY

LEONG MEI KEI

The properties of matter at nanometer scale level are significantly different from their macroscopic bulk properties. Nanomaterials such as metal nanoparticles, carbon nanotube, metal nanowires are viewed as fundamental building blocks for nanotechnology. Metal nanoparticles are presently applied in different fields such as electronics, biotechnology, chemical and biological sensors, DNA labeling, drug delivery, cosmetics, catalysis, environmental remediation, coatings and packaging. Up to now, various physical and chemical methods, have been developed for the synthesis of nanoparticles. However, these methods employ toxic chemicals as reducing agents, organic solvents, or nonbiodegradable stabilizing agents and are therefore potentially dangerous to the environment and biological systems. Moreover, most of these methods entail intricate controls or nonstandard conditions making them quite expensive. Thus, there is a need for “green chemistry” that includes a clean, nontoxic, and environment-friendly method of nanoparticle synthesis. In this study, CuO NPs are synthesized by using Cavendish banana peel extract (BP

extract) as a reducing agent and stabilizing agent. BP extract was prepared with deionized water by heating for 10 minutes and filtered twice, copper nitrate trihydrate was added into the BP extract with continuous boiling until brown precipitate is obtained. Reduction process can be observed with colour change from blue to green. Brown precipitate will be heated in furnace at 400°C for 3 hours. XRD, SEM, FT-IR, EDX and PSA have been used for the characterization of CuO NPs. The photocatalytic activity of CuO NPs has been investigated by degradation of Congo red and Malachite green dye in aqueous solution with exposure to sunlight. The extent of dye degradation by CuO NPs is monitored by using UV-visible spectrophotometer.

ABSTRAK

SINTESIS DAN PENCIRIAN NANOPARTIKEL KUPRUM(II) OKSIDA DAN AKTIVITI FOTOKATALITIK-NYA

LEONG MEI KEI

Pencirian pada skala nanometer adalah jauh berbeza daripada sifat pukal makroskopik mereka. Bahan nano seperti nanopartikel logam, tiub nano karbon, nanowayar logam dilihat sebagai blok binaan asas bagi teknologi nano. Nanopartikel logam masa ini digunakan dalam pelbagai bidang seperti elektronik, bioteknologi, kimia dan sensor biologi, pelabelan DNA, penyampaian ubat, kosmetik, pemangkinan, pemulihan alam sekitar, pelapis dan pembungkusan. Sehingga kini, pelbagai kaedah fizikal dan kimia, telah dibangunkan untuk sintesis nanopartikel. Walau bagaimanapun, kaedah ini menggunakan bahan kimia toksik agen penurunan, pelarut organik, atau agen penstabil, oleh itu berbahaya kepada alam sekitar dan sistem biologi. Selain itu, sebahagian kaedah ini memerlukan kawalan yang rumit atau keadaan yang tidak mengikut piawaian menjadikan mereka agak mahal. Oleh itu, keperluan untuk "kimia hijau" yang merangkumi kaedah yang mudah, kurang toksik, dan mesra alam sintesis nanopartikel semakin mendapat perhatian. Dalam kajian ini, nanopartikel kuprum oksida disintesis dengan menggunakan ekstrak kulit pisang jenis Cavendish (ekstrak BP) sebagai agen penurunan dan agen

penstabil. Ekstrak BP telah disediakan dengan air ternyahion dengan pemanasan selama 10 menit dan ditapis dua kali, kuprum(II) nitrat trihidrat ditambah ke dalam ekstrak BP dengan pemanasan berterusan sehingga pes coklat diperolehi. Proses penurunan dapat dilihat menerusi perubahan warna dari biru ke hijau dan pembentukan pes coklat. Pes coklat akan dipanaskan di dalam relau pada 400 ° C selama tiga jam. XRD, SEM, FT-IR, EDX dan PSA telah digunakan untuk pencirian nanopartikel kuprum(II) oksida. Aktiviti fotokatalitik nanopartikel kuprum(II) oksida telah diperiksa dengan degradasi pewarna merah congo dan hijau malachite dalam larutan akueus di bawah penyinaran cahaya matahari. Tahap degradasi oleh nanopartikel kuprum oksida telah dipantau dengan menggunakan spektroskopi ultra lembayung-cahaya nampak.

ACKNOWLEDGEMENTS

I would like to express my deep sense of gratitude to Dr. Mohammod Aminuzzaman as my final year project supervisor for his valuable guidance and advices at every part of my project. Furthermore, I also offer sincere appreciation for the learning opportunities provided by my FYP supervisor and I came to know about so many new things.

My completion of this final year project could not have been accomplished without the support and help of my lab partner, Mr Wong Hong Liang. I am really thankful to him for giving me a lot of suggestions and inspirations during my project. Furthermore, I want to take this opportunity to thank the lab officers, Mr Leong, Mr Patrick, Mr Hoor and Mr Nicholas for their kind help, supplying glassware and guiding me in handling the instruments. I would like to offer my deep thanks to all of them.

Finally, to my parents and all my friends, I would like to thank them for their endless support and encouragement.

DECLARATION

I hereby declare that the project report is based on my original work except for quotations and citations which have been duly acknowledged. I also declare that it has not been previously or concurrently submitted for any other degree at UTAR or other institutions.

Leong Mei Kei

Date:

APPROVAL SHEET

I hereby certify that, this project report entitled “**GREEN SYNTHESIS, CHARACTERIZATION OF COPPER(II) OXIDE NANOPARTICLES AND THEIR PHOTOCATALYTIC ACTIVITY**” was prepared by **LEONG MEI KEI** and submitted in partial fulfilment of the requirements for the degree of Bachelor of Science (Hons.) in Chemistry at Universiti Tunku Abdul Rahman.

Approved by

Supervisor

Date: _____

(Asst. Prof. Dr. Mohammod Aminuzzaman)

Department of Chemical Science

Faculty of Science

Universiti Tunku Abdul Rahman

FACULTY OF SCIENCE
UNIVERSITI TUNKU ABDUL RAHMAN

Date: _____

PERMISSION SHEET

It is hereby certified that **LEONG MEI KEI** (ID No: **13ADB07176**) has completed this report entitled **“GREEN SYNTHESIS, CHARACTERIZATION OF COPPER(II) OXIDE NANOPARTICLES AND THEIR PHOTOCATALYTIC ACTIVITY”** under supervision of **ASST. PROF. DR. MOHAMMOD AMINUZZAMAN** from the Department Chemical Science, Faculty of Science.

I hereby give permission to my supervisor to write and prepare manuscript of these research findings for publishing in any form, if I did not prepare it within six(6) month time.

Yours truly

(Leong Mei Kei)

TABLE OF CONTENTS

	Page
ABSTRACT	ii
ABSTRAK	iv
ACKNOWLEDGEMENTS	vi
DECLARATION	vii
APPROVAL SHEET	viii
PERMISSION SHEET	ix
LIST OF TABLES	xiii
LIST OF FIGURES	xiv
LIST OF ABBREVIATIONS	xvii
CHAPTER	
1. INTRODUCTION	1
1.1 Background of study	1
1.2 Nanoparticles	2
1.3 Metal nanoparticles, Copper(II) oxide, CuO	6
1.4 Synthesis of CuO NPs	6
1.5 Photocatalytic activity of CuO NPs	10
1.6 Objectives	12

2.	LITERATURE REVIEWS	13
2.1	Nanoparticles, CuO NPs	13
2.2	Green synthesis of CuO nanoparticles	14
2.2.1	Nanoparticles synthesis using plant extract	15
2.2.2	Nanoparticles synthesis using fruit extract	22
2.2.3	Nanoparticles synthesis using microorganism	24
2.3	Previous studies of CuO NPs on photocatalytic dye degradation	31
3.	METHODOLOGY	33
3.1	Chemicals	33
3.2	Green synthesis of CuO NPs	33
3.2.1	Preparation of Cavendish banana peel extract (BPE)	33
3.2.2	Synthesis process of CuO NPs	34
3.3	Characterization of synthesized CuO NPs	35
3.4	Calculation of crystalline size using Debye-Scherrer equation	36
3.5	Preparation of Congo red and Malachite green dye solution	37
3.6	Degradation study on Congo red and Malachite green using CuO NPs as function of time	37
3.7	Determination of degradation percentage	39
4.	RESULTS AND DISCUSSION	40
4.1	Synthesis of CuO nanoparticles	40
4.2	Characterization of CuO NPs	42
4.2.1	X-ray Diffraction	42
4.2.2	Energy-dispersive X-ray Spectroscopy	43

4.2.3 Fourier Transform Infrared Spectroscopy	44
4.2.4 Scanning Electron Microscopy	46
4.2.5 Particle Size Analyzer	47
4.3 Degradation of dye solution by CuO NPs	48
4.3.1 Congo red dye degradation	48
4.3.2 Malachite green dye degradation	52
4.3.3 Degradation rate of Congo red and Malachite green dye solution	57
5. CONCLUSION	58
REFERENCES	60
APPENDICES	72
A. Information of crystallinity of CuO NPs	72
B. Calculation of crystalline size using Debye-Scherrer Equation	73
C. Degradation percentage of Congo red as a function of contact time.	74
D. Degradation percentage of Malachite green as a function of contact time.	75
E. XRD information of synthesized nanoparticles (Part I)	76
F. XRD information of synthesized nanoparticles (Part II)	77
G. Synthesized CuO NPs, JCPDS 048-1548	78

LIST OF TABLES

Table		Page
1.1	Applications of nanoparticles	5
1.2	List of different metal nanoparticles synthesized from various plant extracts.	8
1.3	List of different metal nanoparticles synthesized from various microorganisms.	9
4.1	Crystalline sizes and average particle sizes of CuO NPs.	47

LIST OF FIGURES

Figure		Page
1.1	Top-down and Bottom-Up approaches in synthesizing nanoparticles.	3
1.2	A series of photodegradation equations of dye molecules by CuO NPs.	11
1.3	Illustration of photocatalytic degradation process of CuO NPs.	11
2.1	Biosynthesis and applications of metal nanoparticles.	15
2.2	Flow chart of nanoparticles synthetic pathway using plant as green source.	16
2.3	<i>Gloriosa superba</i> L.	17
2.4	(a) UV-Vis spectra of CuO NPs of different amount of plant extract used. (b) SEM and (c) TEM images of CuO NPs.	17
2.5	<i>Cassia alata</i> L.	18
2.6	XRD spectrum of copper oxide nanoparticles (left) and SEM images of copper oxide nanoparticles (right).	19
2.7	(a) UV-Vis spectra and (b) FTIR spectra of CuO NPs.	20
2.8	(a) SEM and (b) TEM images of CuO NPs synthesized using <i>Aloe vera</i> extract.	20
2.9	(a) UV-vis comparison spectrum of <i>Bifurcaria bifurcata</i> extract and CuO NPs, (b) FTIR spectrum, (c) XRD pattern analysis and (d) TEM image of CuO NPs.	22
2.10	UV-vis spectra of synthesis of CuO NPs from lemon extract.	23
2.11	(a) SEM image, (b) TEM image and (c) XRD pattern of synthesized CuO NPs.	24
2.12	(a) UV-vis absorption spectra, (b) particle sizes distribution based on DLS analysis and (c) SEM image of CuO NPs using extract of <i>E.coli</i> .	25

2.13	TEM image (top left), UV-Vis spectra (bottom left) and XRD pattern of synthesized CuO NPs (right).	26
2.14	(A) UV-Vis spectra of reducing protein that presence in (a) <i>Penicillium citrinum</i> , (b) <i>Penicillium waksmanii</i> and (c) <i>Penicillium aurantiogriseum</i> . (B) DLS analysis. (C) SEM images for CuO NPs synthesis by using <i>Penicillium citrinum</i> , <i>Penicillium waksmanii</i> and <i>Penicillium aurantiogriseum</i> (from left to right). (D) AFM image of CuO NPs.	28
2.15	(a) UV-vis spectra synthesis reaction time of 24 h, 36h and 42 h, (b) XRD pattern, (c) TEM image, (d) SEM image of synthesized CuO NPs and (e) EDX spectrum recorded for incubated <i>Phormidium cyanobacterium</i> with copper sulphate for 42 h.	30
3.1	Schematic diagram of synthesis process of CuO NPs.	35
4.1	Synthesized CuO NPs.	41
4.2	XRD pattern of synthesized CuO NPs.	42
4.3	EDX spectrum of CuO NPs.	43
4.4	FT-IR comparative spectrum of synthesized CuO NPs and BPE.	44
4.5	SEM images of CuO NPs with different magnifications X=13000, 22000 and 45000.	46
4.6	Size distribution histogram of CuO NPs.	47
4.7	Molecular structure of Congo Red.	49
4.8	UV-Vis spectra of Congo red dye degradation as a function of time.	51
4.9	Decolourization of Congo red solution at different time intervals.	51
4.10	Degradation percentage of Congo red at different time intervals.	52
4.11	Molecular structure of Malachite green.	53
4.12	Tentative photocatalytic mechanism of Malachite green	54

4.13	UV-Vis spectra of Malachite green dye degradation as a function of time.	55
4.14	Decolourization of Malachite green solution at different time intervals.	55
4.15	Malachite green dye solution before and after degradation.	56
4.16	Degradation percentage of Malachite green at different time intervals.	56

LIST OF ABBREVIATIONS

Å	Angstrom
A ₀	Initial absorbance of dye solution
A _t	Absorbance of dye solution at reaction time, t
AFM	Atomic Force Microscopy
Ag	Silver
Au	Gold
BPE	Banana peel extract
cm ⁻¹	Wavenumber
C	Carbon
CB	Conduction band
CO	Carbon monoxide
CO ₂	Carbon dioxide
CR	Congo red
Cr(IV)	Chromium(IV)
Cu	Copper
CuO	Copper(II) oxide
Cu ₂ O	Cuprous oxide
CuO NPs	Copper oxide nanoparticles
D	Crystalline size in diameter
DLS	Dynamic Light Scattering
e ⁻	Electron
EDX	Electron-dispersive X-ray spectroscopy
eV	Electron volt
Fe	Iron
FT-IR	Fourier Transform Infrared
FWHM	Full-width half maximum
g	Gram
GC-MS	Gas-chromatography-mass spectrometry

h^+	Hole
H^+	Hydrogen ion
h	Plank constant
H_2O	Water
Hg	Mercury
H_2O_2	Hydrogen peroxide
JCPDS	Joint Committee on Powder Diffraction Standards
k	Shape factor
kV	Kilovolt
LC-MS	Liquid chromatography-mass spectrometry
mA	Milliampere
MB	Methylene blue
MG	Malachite green
Mg	Magnesium
mg	Milligram
mL	Millilitres
MO	Methylene orange
mW	Milliwatt
Na	Sodium
nm	Nanometer
O	Oxygen element
O_2	Oxygen molecule
O_2^-	Super oxide anion
OH^-	Hydroxide
OH^*	Hydroxyl radical
Pd	Palladium
pH	Potential of hydrogen
PSA	Particle Size Analyser
Pt	Platinum
ppm	Parts per million

rpm	Revolutions per minute
S	Sulphur
Se	Selenium
SEM	Scanning Electron Microscopy
SEM-EDS	Scanning Electron Microscopy with X-ray Microanalysis
TEM	Transmission Electron Microscopy
TiO ₂	Titanium dioxide
UV	Ultraviolet
UV-Vis	Ultraviolet-visible
VB	Valence band
XRD	X-ray Diffraction
ZnO	Zinc oxide
θ	Diffraction angle
λ	Wavelength of X-ray source or lambda
λ_{\max}	Maximum wavelength
π	Pi
α	Alpha
β	Width of a diffraction peak at full-width half maximum or beta
ν	Frequency
°C	Degree Celsius

CHAPTER 1

INTRODUCTION

1.1 Background of study

The Greatman Richard Feynman (American physicist, 1918-1988) was the first scientist who raised a discussion on atomic scale technology. In 1959, Richard Feynman delivered a speech entitled “There’s Plenty of Room at the Bottom” which emphasized on the problem of controlling things on small scale. In 1974, Professor Norio Taniguchi (1912-1999) coined the term “nanotechnology” to describe precision machining materials on nanometer dimensions. In the 1981s, IBM scientists invented the scanning tunnelling microscope which can create images of the individual atoms. Invention of scanning tunnelling microscope has become one of the significant milestones for nanotechnology development. In 1986 atomic force microscope was invented to measure and manipulate size of materials at nanometer scale. Dr K. Eric Drexler published his first book: Engines of Creation: The Coming Era of Nanotechnology. In the late twentieth century, usage of nanotechnology in medical sciences and engineering has becoming more and more prevalent. Because of its technological and economical values, nanotechnology has been penetrated as a key industry after 2002-2003. (Roco, 2011)

Nanoscience and nanotechnologies are the newly arisen interdisciplinary approaches to research and development related to the manipulation of fundamental structure and matter's behaviour at atomic and molecular levels. (International Iberian Nanotechnology Laboratory, n.d.). In fact, nanotechnology can be defined as the study and control of materials whose particles size lie between 1-100 nm at any of their dimensions. Emergence of nanotechnology as a rapid growing sector with its widespread applications in both science and technologies areas has attracted a lot of researches from many other fields. Materials that reduced to nanoscale are unique as they exhibit optical, electronic, magnetic, physical and chemical properties that are totally different from bulk materials. The properties of nanomaterials change considerably as particles size vary. There is a size scale called quantum effects that govern the behaviour and properties of the nanoparticles whereas for bulk materials, physical properties will not be affected by its size.

1.2 Nanoparticles

Nanoparticles can be formed by two approaches: top-down (comminution and dispersion) or bottom-up (nucleation and growth). (Ramsden, 2009) Top-down approach is making use of the starting bulk materials of the same materials that going to be synthesized and applying energy to break down the large materials into smaller fragments. Sources of energy can be mechanical, thermal or chemical. However, there is an disadvantage associated with this method whereby this will be creating particles with wide size distribution. To

overcome this, Bottom-up method was introduced as it is considered simpler and more favourable in synthesizing nanoparticles in size less than 100 nm whereby it was like building the atoms one by one, first started with a simple metal salt, slowly converts it from ions to elemental atoms by chemically eventually clumped and grown in the form of nano-size particles. The synthesizing process was illustrated as below:

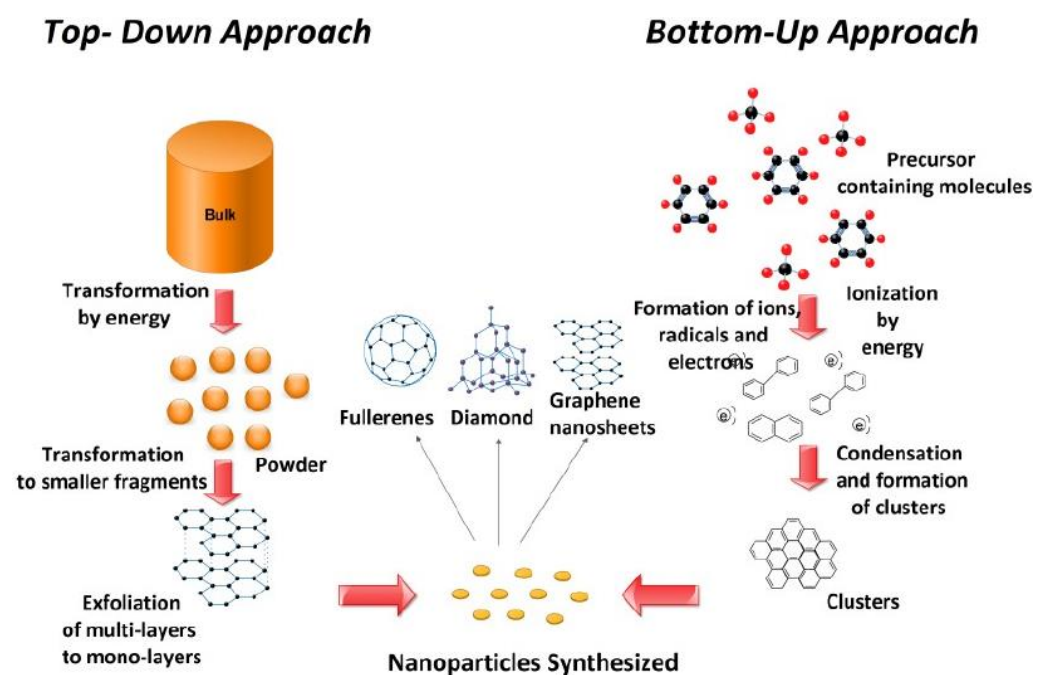


Figure 1.1: Top-down and Bottom-Up approaches in synthesizing nanoparticles. (Habiba, et al., 2014)

In fact, nanoparticles do exhibit special properties which are significantly different from their bulk materials. In terms of physical properties, nanoparticles are having larger surface area compared to those of macroscale materials which making them to exhibit lower melting point. For instance, gold nanoparticle melts at approximately 300°C for particle size of 2.5 nm which is

lower than its bulk substitute that melts at 1064°C. On the other hand, nanoparticles possess optical properties due to the quantum effects and their ability in confining electrons. Gold nanoparticles change from deep red to black when it is in solution, bulk gold appears in yellow colour. Another significant physical property that makes nanoparticles so special is their ability to form suspension. Formation of suspension is possible by strong interaction between particle surface and solvent to overcome the density difference of the two mediums meanwhile suspension in bulk material is not favorable where it may be either sinking or floating in the solution.

With the use of nanotechnology, more advanced and improved goods are produced by taking advantage of modifying the materials at nanoscale as physical properties of nanomaterials are size-dependent. Nanoparticles are now utilized and exploited for a potential use in medicine, environment, food, heavy industry and consumer goods as shown in Table 1.1.

Table 1.1: Applications of nanoparticles. (Progetti, 2016)

Fields	Applications
Medicine	<ul style="list-style-type: none"> - as a drug deliver to targeted cells. - nanoparticles carry chemotherapy drugs to the infected cancer cells so that it will not cause any damage to healthy cells.
Environment	<ul style="list-style-type: none"> - used for removal of traces of metal (copper, lead and mercury) and biological substances (viruses, parasites etc). - commonly used in wastewater treatment due to its high surface area to volume ratio. (Tiwari, Behari and Sen, 2008)
Food	<ul style="list-style-type: none"> - applied on manufacturing, processing and packaging of food. - nanocomposite coating used to improve mechanical and heat resistance.
Heavy industry	<ul style="list-style-type: none"> - nanotech materials used in aircraft manufacturing, to decrease fuel consumption due to its lightweight and toughness. - nanocoating helps to protect the surface of aircraft from unfavourable weather condition.
Consumer goods	<ul style="list-style-type: none"> - Titanium dioxide (TiO₂) and zinc oxide (ZnO) nanoparticles are incorporated in many sunscreen products because of their excellent UV blocking properties. (Kessler, 2011)

1.3 Metal nanoparticles, Copper(II) oxide, CuO

Metal oxides are the most diverse group in chemistry as their special properties covered nearly all aspects in both science and technology. Among various metal oxides, transition metal oxides are the most technologically advanced and economically attractive. (Kung, 1989) Copper oxides nanoparticles (CuO NPs) are of interest because it is simple, high stability, relatively more cost effective than other metals like gold and silver, stable over a wide range of pH and high temperature resistance. CuO NPs is one of the metal oxides which were found to be extremely useful in wide variety of applications due to their uniqueness. CuO NPs were extensively utilized as antimicrobial agent (Ren, et al., 2009), photocatalyst (Katwal, et al., 2015), solar cells (Kidowaki, et al., 2012), lithium ion battery (Thi, et al., 2014) and gas sensor (Zhang, et al., 2011)

1.4 Synthesis of CuO NPs

Copper oxide nanoparticles can be synthesized by various chemical methods such as sol-gel method (Etefagh, Azhir and Shahtahmasebi, 2013), precipitation (Phiwdang, et al., 2013), hydrothermal synthesis (Outokesh, et al., 2011), chemical reduction, thermal decomposition, electrochemical method (Ghorbani, 2014) and wet chemical method. (Joshua, et al., 2014) Conventional chemical methods for nanoparticles synthesis are associated with various disadvantages such as expensive, involved the use of chemicals, time

consuming and pose environmental threats by generating toxic solvent and waste products (Zhou, et al., 2010) which leads to a growing need to develop greener, environmentally friendly approach in synthesizing the metal nanoparticles. (Khalil, et al., 2014) It has been reported that many of the biological systems such as bacteria, fungi, algae, plants and human cells can be used to convert metal ions into metal nanoparticles. (Makarov, et al., 2014) According to the 12 principles of green chemistry, synthesis of nanoparticles by using plant extract and microorganism has an advantage over conventional methods. (Devi and Singh, 2014) This approach provides a safer alternative to produce nanoparticles with desired physical and chemical properties. However, there are certain limitations to be taken note of during synthesis part as different synthesis methods could give different types of nanoparticles. Firstly, the size and shape of nanoparticles formed depends on the types of green synthesizer used, different amount of extract used, experiment parameters and these factors could lead to subsequent changes in nucleation process and number of functional groups deposited on the existing nanoparticles surface to avoid agglomeration. Tables 1.2 and 1.3 listed out the use of various plants and microorganisms used in synthesizing metal nanoparticles.

Table 1.2: List of different metal nanoparticles synthesized from various plant extracts.

Plant materials	Synthesized nanoparticles	References
<i>Medicago sativa</i> (leaf extract)	Ag	(Gardea, et al., 2003).
<i>Geranium indicium</i> (leaf extract)	Ag	(Shankar, et al., 2003).
<i>Carica papaya</i> (callus extract)	Ag	(Mude, et al., 2009).
<i>Avena sativa</i> (biomass)	Au	(Armendariz, et al., 2004).
<i>Aloe vera</i> (leaf extract)	Au	(Chandran, et al., 2006).
<i>Alfa alfa</i> (powder milled)	Fe	(Herrera-Becerra, et al., 2008).
<i>M. kobus</i> (leaf extract)	Cu	(Lee, et al., 2011).
<i>T. procumbens</i> (leaf extract)	Cu	(Gopalkrishnan, et al., 2012).
<i>Physalis alkekengi</i> (plant extract)	Zn	(Qu, et al., 2011).
<i>Anacardium occidentale</i> (dried leaf powder)	Pd	(Sheny, Philip and Mathew, 2012).

Table 1.3: List of different metal nanoparticles synthesized from various microorganisms.

Microorganisms	Synthesized nanoparticles	References
<i>Sargassum wightii</i>	Au	(Li, et al., 2011).
<i>Rhodococcus</i> sp.	Au	(Ahmad, et al., 2003).
<i>Escherichia coli</i>	Au	(Du, et al., 2007).
<i>Yarrowia lipolytica</i>	Au	(Agnihotri, et al., 2009).
<i>Brevibacterium casei</i>	Ag, Au	(Kalishwaralal, et al., 2010).
<i>Trichoderma viride</i>	Ag	(Mohammed, Balaji and Venkatesan, 2009).
<i>Shewanella algae</i>	Pt	(Konishi, et al., 2007).
<i>Enterobacter</i> sp	Hg	(Sinha and Khare, 2011).
<i>Shewanella</i> sp	Se	(Lee, et al., 2007).
<i>Desulfovibrio desulfuricans</i>	Pd	(Lloyd, Yong and Macaskie, 1998).

Green synthesis of nanoparticles has been accomplished by making use of plant extract as an eco-friendly and natural resource functions as reducing agent as well as capping agent. In this project, synthetic pathway of CuO NPs was carried out by using Cavendish banana peel. Nowadays, fruit peels are commonly used as a natural source containing high content of antioxidants and phytochemical constituents which are highly active in free radical scavenging activity. These components will be responsible for reducing the metal salt to metal and further oxidized in air to metal oxide nanoparticles. Banana peels are the major agriculture waste resulted from food waste as people thrown the peel away after consumed the pulp, it also applied in soap making, leather processing and medicine. More importantly, banana peels are found to be a source of antioxidants and phenolic compounds, for example, gallic acid (Someya, Yoshiki and Okubo, 2002) and dopamine (Kanazawa and Sakakibara, 2000).

1.5 Photocatalytic activity of CuO NPs

In this study, CuO NPs will be used as a photocatalyst for photodegradation of commercial dye solution which utilizing sunlight energy as a natural energy supply. CuO NPs is a well-known p-type conductor along with narrow band gap of 1.2 eV. (Yao, et al., 2010) Basically, photocatalytic activity of CuO NPs was being evaluated by measuring extent of dye solution being degraded. The possible mechanism of dye degradation was proposed as follows:

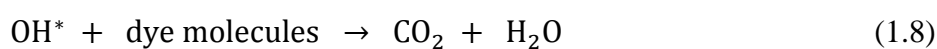
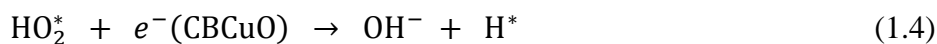
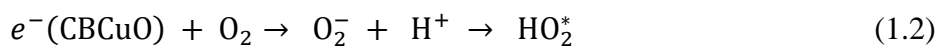
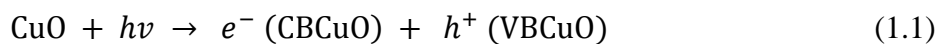


Figure 1.2: A series of photodegradation equations of dye molecules by CuO NPs. (Wei, et al., 2013; Sharma and Sharma, 2012; Katwal, et al., 2015)

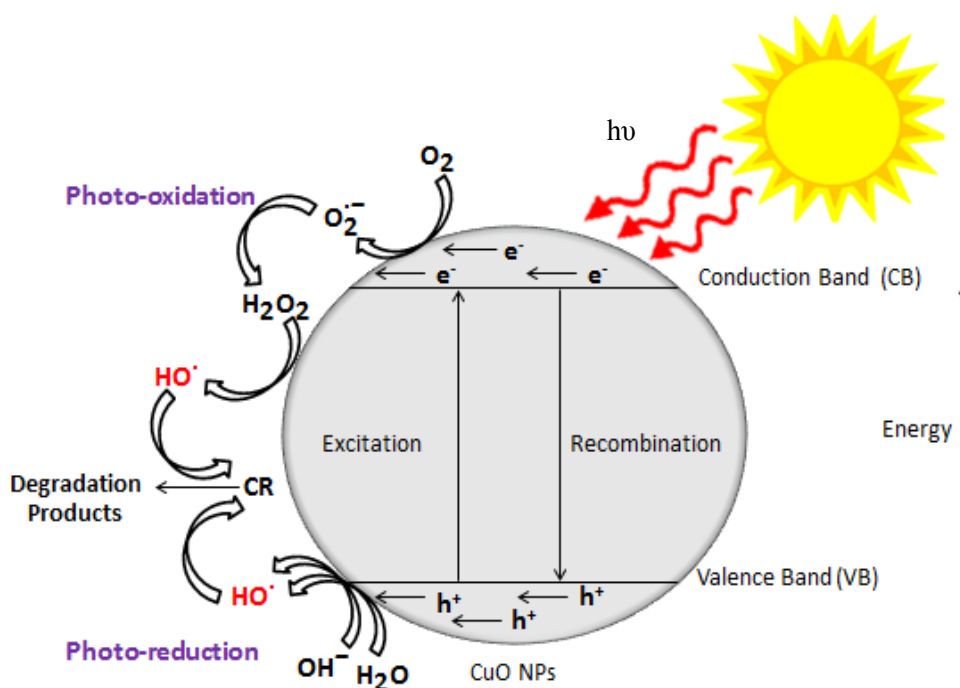


Figure 1.3: Illustration of photocatalytic degradation process of CuO NPs. (Sharma and Sharma, 2012; Saikia, et al., 2015)

In the photocatalytic reaction, CuO as a semiconductor material will absorb the sunlight energy equal or higher than its band gap energy thus leading to the excitation of electron from valence band (VB) to the conduction band (CB). As a result, a vacancy was created at valence band which labelled as h^+ while excited electron at conduction band was symbolized as e^- . Pair of electron (e^-) and hole (h^+) was generated. This stage is called photo-excitation stage. The vacancies (holes) react with water to form hydroxyl radicals (OH^\cdot). At the same time, electrons react with oxygen to form a series of oxidizing species like super oxide anion, hydrogen peroxide and hydroxyl radicals. The cycle will continue in the presence of sunlight.

1.6 Objectives

1. To synthesize CuO NPs using Cavendish banana peel extract (BPE) by green synthetic pathway.
2. To characterize CuO NPs using Fourier Transform Infrared Spectrometer (FT-IR), X-Ray Diffraction (XRD), Scanning Electron Microscopy (SEM), Energy Dispersive X-Ray Spectroscopy (EDX) and Particle Size Analyser (PSA).
3. To evaluate photocatalytic activity of CuO NPs in the degradation of Congo Red (CR) and Malachite green (MG) dye solution under solar irradiation.

CHAPTER 2

LITERATURE REVIEWS

2.1 Nanoparticles, CuO NPs

Nanotechnology is one of the branches in science and technology fields which utilize the materials in the size of 1-100 nm which come with different shapes such as spherical, rods, ribbons, platelets and belt. Copper oxide is a compound of two copper and an oxygen element. Copper oxide can be referred to as tenorite (CuO) and cuprite (Cu₂O). (Alabi, et al., 2013) CuO NPs are categorized under monoclinic structure system. (Suleiman, et al., 2013) CuO NPs exhibit optical, electrical, mechanical and catalytic properties leads to applications in the field of superconductors, catalysis and ceramic as an inorganic material. The high surface-to-volume ratio property leads to possession of unique chemical and physical properties which makes them so different from the micro or bulk size materials. This is because the size of nanoparticles are much more smaller than the bulk materials, large surface area could give efficient adsorption of organic dye molecules in the first stage of dye removal. It was proven that nano-sized copper oxide shows superior catalytic activity as compared to ordinary copper oxide. Meanwhile different shapes and sizes of nanoparticles are exploited in different uses accordingly. For instance, copper oxide nanofluids found out to be having 12.4 % higher

thermal conductivity relative to deionised water (Manimaran, et al., 2013), while various nanocrystallite shapes of CuO giving different catalytic reactivity in oxidizing process of CO. Effect of different shapes of CuO was investigated as nanoplatelets are more easily being reduced where it convert CO to CO₂ at 77°C and 134°C. On the other hand, conversion of CO by nanobelts and nanoparticles happened at higher temperature 90°C and 194°C. (Yao, et al., 2005)

2.2 Green synthesis of CuO nanoparticles

Due to the wide applications in diverse branches of advanced scientific fields, more and more researchers have been focused on the synthesis of CuO NPs in different routes. The brief review of synthesis of CuO NPs was described as below. Metal salt of corresponds metal nanoparticles going to be synthesized was chosen as the precursor in preparation of nanoparticles. They were reduced to metal ions in the presence of bioactive functional groups present in the natural sources (acting as a natural reducing agent).

Figure 2.1 illustrated various environmentally benign materials like plant extracts (stem, flowers, seed, root, and fruits), bacteria, fungi and enzymes are employed in synthesis pathway of metal nanoparticles for the purpose of eco-friendliness and utilized for pharmaceutical and other biomedical applications as it is free of toxic chemicals. (Jain, et al., 2009)

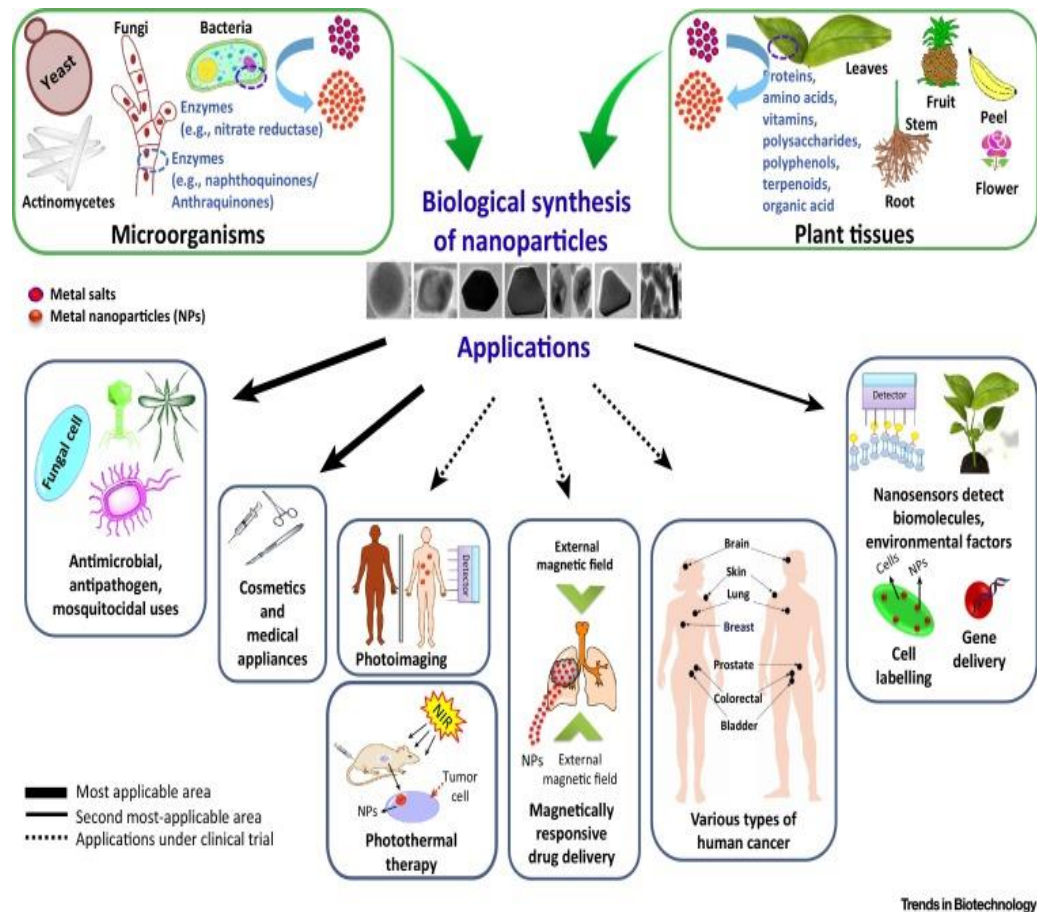


Figure 2.1: Biosynthesis and applications of metal nanoparticles. (Singh, et al., 2016)

2.2.1 Nanoparticles synthesis using plant extract

Phytonanotechnology has become an upcoming new area of research for biological synthesizing method of metal nanoparticles. Plant extract is far more advantageous with the present of functional components in plants which can be used as a reducing agent and capping agent as well. This is a better method as they give excellent manipulation on controlling the particle size growth thus provide considerably stabilization during synthesizing process. (Prasad, 2014) By making use of plant extract, specific nanoparticles with desired size and

shape can be designed for wide variety of nanotechnological applications. Various parts of the plants can be used for synthesis of metal nanoparticles including leaves, stems, roots and seeds. It has been reported that the phytochemicals, primary and secondary metabolites are well known as natural resources that responsible for metal salt reduction. (Baker, et al., 2013) The degree of accumulation of metal nanoparticles is influenced by the reducing power of the plant extract with the reacting metal ion's oxidation state. Figure 2.2 showed the process of synthesis and characterization of nanoparticles.

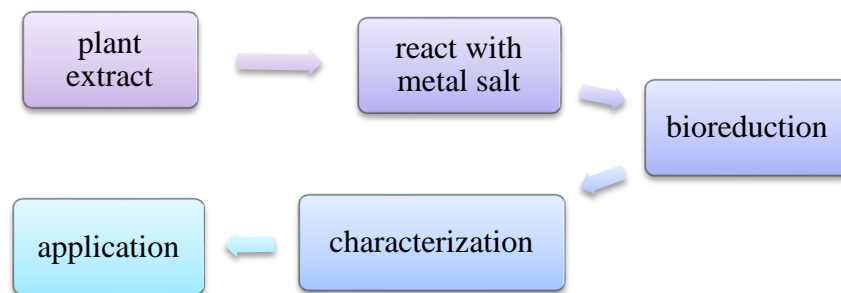


Figure 2.2: Flow chart of nanoparticles synthetic pathway using plant as green source. (Sen, Prakash and De, 2015)

Naika, et al., 2015 reported the synthesis of copper oxide nanoparticles by using *Gloriosa superba* L. extract. 1 mL of *Gloriosa superba* L. leaves extract was added to cupric nitrate with small amount of distilled water. The mixture was stirred constantly and heated in furnace at 400°C. CuO NPs was formed within 3-4 minutes.



Figure 2.3: *Gloriosa superba* L. (Choudhary, 2016)

In this review, effect of different concentration of plant extract on the size and structure of particles were evaluated. It has been proven that structure of particle is not affected by amount of plant extract used. From the XRD result, the particles were monoclinic in nature while SEM image showed that the shape of particles is spherical in shape which indicates that the particles were uniformly distributed. In addition, TEM image revealed that CuO nanoparticles were found out to be in the range 5-10 nm.

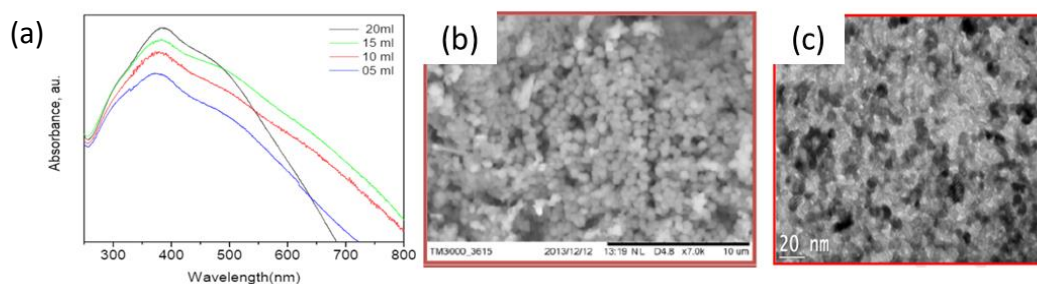


Figure 2.4: (a) UV-Vis spectra of CuO NPs of different amount of plant extract used. (b) SEM and (c) TEM images of CuO NPs. (Naika, et al., 2015)

Another research by Jayalakshmi and Yogamoorthi, 2014, they are using flower of *Cassia alata* to synthesis CuO NPs, *Cassia alata* L. is belong to family Fabaceae which reported to have phytochemical activity.



Figure 2.5: *Cassia alata* L. (Jayalakshmi and Yogamoorthi, 2014)

Cassia alata has been analysed to contain active anthraquinones such as rhein, emodin, physcion and flavonoid. (Chatterjee, 2013) Furthermore, Akthar, Birhanu and Demisse, 2014 also reported that the preliminary phytochemical screening test on this plant showed the presence of anthraquinone, sapoin, phenolic compounds and flavonoids. All of these can act as bioreductant in nanoparticles synthesis. SEM scanning showed the size was 110-280 nm and the surfaces of particles were rough. Other than that, UV-Vis spectroscopy was used to characterize the nanoparticles as well. As a result, a single broad peak was obtained at 263 nm. XRD analysis was done to observe the crystalline cubic phase of monoclinic copper oxide.

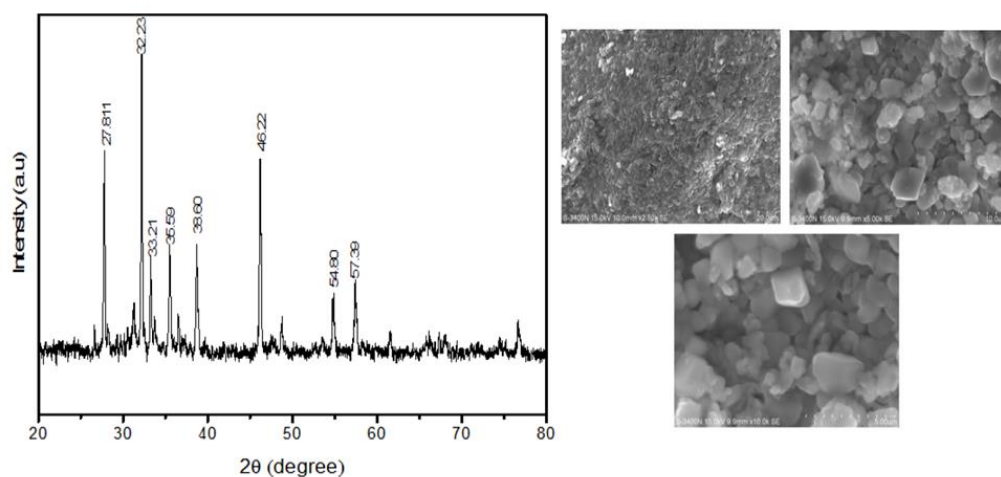


Figure 2.6: XRD spectrum of copper oxide nanoparticles (left) and SEM images of copper oxide nanoparticles (right). (Jayalakshimi and Yogamoorthi, 2014)

A study by Kumar, et al., 2015, reported the use of aloe vera leaf extract for green synthesis of nanoparticles. Aloe vera is a therapeutic plant that can be used for medicinal purposes for treatment of human disease. As findings from Raphael, 2012, aloe vera was found out to be abundance with phytochemical constituents such as tannins, flavonoids, terpenoids and alkanoids that can be fully utilized as bio-reductance. This hypothesis was supported by Dinesh, Patel and Dhanabal, 2012, claiming that aloe vera contains huge amount of phenolic compounds, glycosides, 1,8-dihydroxyanthraquinone derivatives (emodin) and beta-1,4 acetylated mannan. CuO NPs were characterized by FT-IR, SEM-EDS, XRD, TEM and UV-Vis spectroscopy. As from the IR spectrum, peaks appeared at 529 and 350 cm^{-1} can be assigned to CuO vibrations. Two strong resonances in UV spectra were showed between 265 nm to 285 nm. Formation of CuO NPs was confirmed by appearance of another weak broad peak at about 670 nm. Furthermore, XRD spectrum indicated

monoclinic structure of CuO NPs and estimated crystalline size was about 22 nm. On the other hand, agglomeration and overlapping of particles were observed on SEM image giving a particle size of 100 nm approximately. Thus synthesized CuO NPs was being subjected to TEM to obtain an exact particle size of each of the single particle alone. As a result, CuO NPs was found out to be in the range of 20-30 nm.

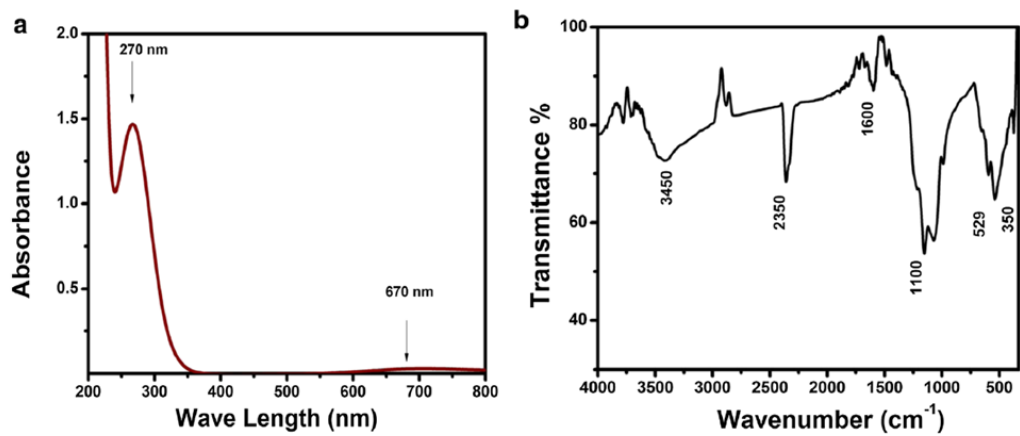


Figure 2.7: (a) UV-Vis spectra and (b) FTIR spectra of CuO NPs. (Kumar, et al., 2015)

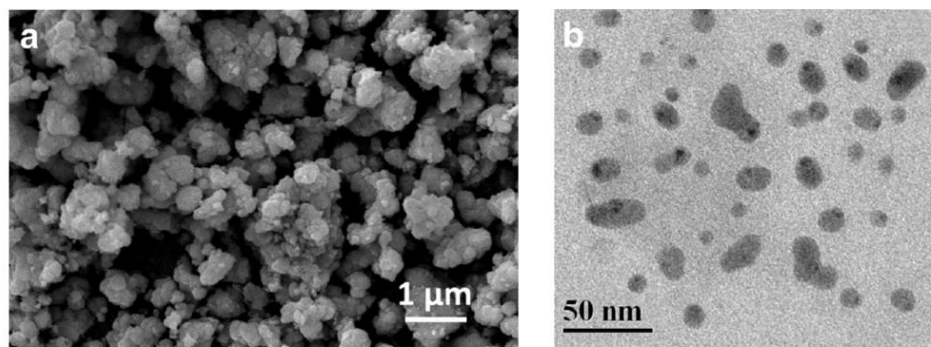


Figure 2.8: (a) SEM and (b) TEM images of CuO NPs synthesized using *Aloe vera* extract. (Kumar, et al., 2015)

Another research on synthesis of CuO NPs by using *Bifurcaria bifurcata*, a brown alga and their antimicrobial activity was done by Abboud, et al., 2014. CuO NPs were further studied for antimicrobial activity against *Enterobacter aerogenes* (gram-negative) and *Staphylococcus aureus* (gram-positive). *Bifurcaria bifurcata* was found to be having excellent antioxidant activity with the presence of phenolic compounds. (Zubia, et al., 2009) Synthesized CuO NPs was confirmed by many techniques such as UV-visible spectroscopy, XRD, TEM and FT-IR. As shown by comparison UV-Vis spectrum, a control (brown alga extract) having two peaks at 245 nm and 290 nm correspond to diterpenoids compounds this related to previous studies by (Daoudi, et al., 2001); (Munoz, Culioli and Kock., 2012); (Combaut and Piovetti, 1983); (Valls, et al., 1993); (Culioli, et al., 2004) stating that acyclic diterpenes was found abundance in *Bifurcaria bifurcata* species. On the other hand, the UV-Vis spectrum for mixture of copper sulphate and brown alga extract showed two strong peaks at 260 nm assigned to cuprous oxide nanoparticles and 650 nm assigned to cupric oxide nanoparticles. TEM illustrated the size and shape of single nanoparticles itself. It was observed that mostly are in spherical shape and a few exist in rod shape. The particle size was in the range of 5-45 nm. XRD pattern implied that there are mixture of monoclinic cupric oxide (CuO) and cubic cuprous oxide (Cu₂O). FT-IR spectra of *Bifurcaria bifurcata* and CuO NPs were compared. Disappearance of C=O band at 1730 cm⁻¹ indicates the reduction of copper ions has been taken place by diterpenoids presence in *Bifurcaria bifurcata*. This was in accordance with UV-visible spectra discussed earlier.

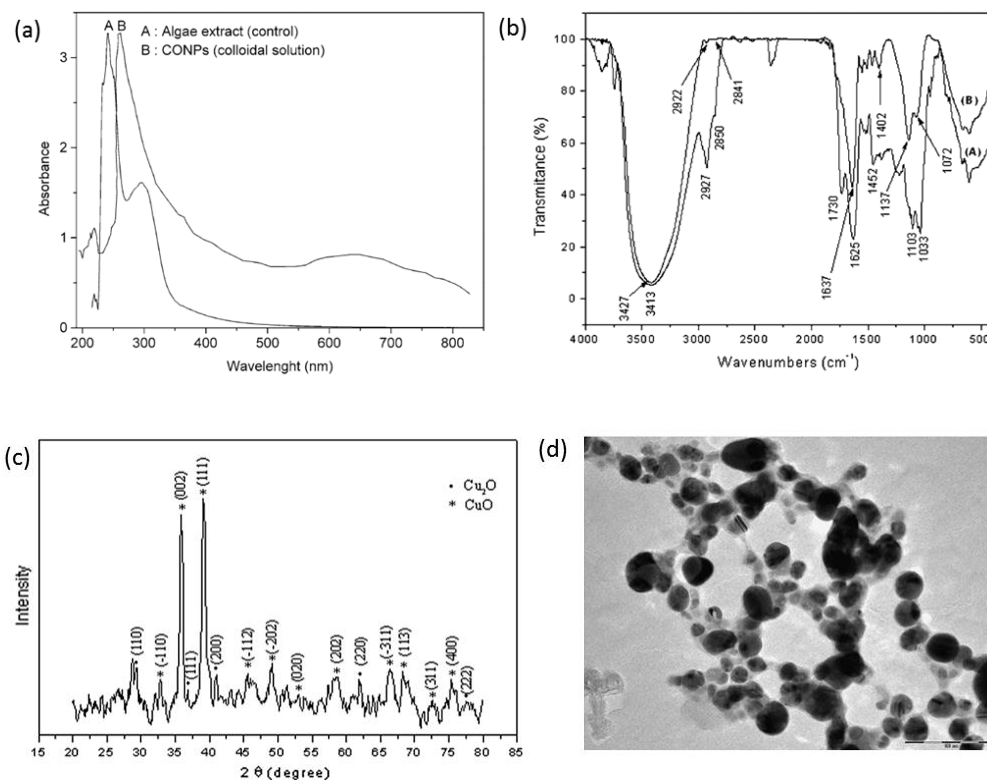


Figure 2.9: (a) UV-vis comparison spectrum of *Bifurcaria bifurcata* extract and CuO NPs, (b) FTIR spectrum, (c) XRD pattern analysis and (d) TEM image of CuO NPs. (Abboud, et al., 2014)

2.2.2 Nanoparticles synthesis using fruit extract

Citrus juices are well known to contain numerous bioactive compounds such as phenolics, flavonoids, vitamins and essential oils that responsible for antioxidative, anti-inflammatory and antimicrobial activities. (Oikeh, et al., 2016) This finding was similar to the research done by Mathew, Jatawa and Tiwari, 2012 declared that extract of lemon pulp has high content of alkaloids, tannins, reducing sugars, phenols and flavonoids. CuO NPs have been synthesized by using *citrus* limon juice and studied on its application as

nanosorbent for Cr(IV) remediation. (Mohan, et al., 2015) According to the research, synthesized CuO NPs was interpreted by UV-Vis absorption spectroscopy as shown.

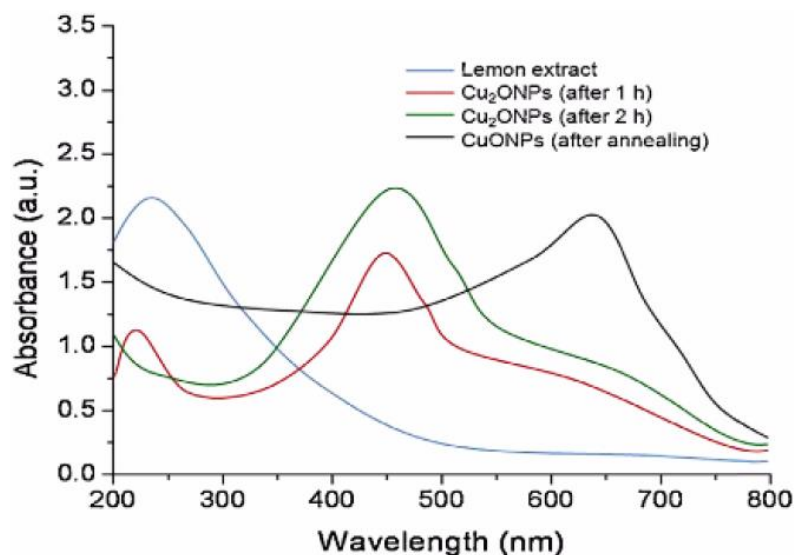


Figure 2.10: UV-vis spectra of synthesis of CuO NPs from lemon extract. (Mohan, et al., 2015)

The spectra were recorded at two different time intervals (after 1 hour and 2 hours) during the first stage of synthesis and followed by annealing for another 2 hours to convert the Cu₂O NPs to CuO NPs completely. On the other hand, SEM image showed the particles were all uniformly distributed with spherical shape and TEM image revealed the average particles size was in the range of 5-20 nm. A XRD pattern of CuO NPs was observed and determined the average crystalline size of CuO NPs was 94.1428 Å.

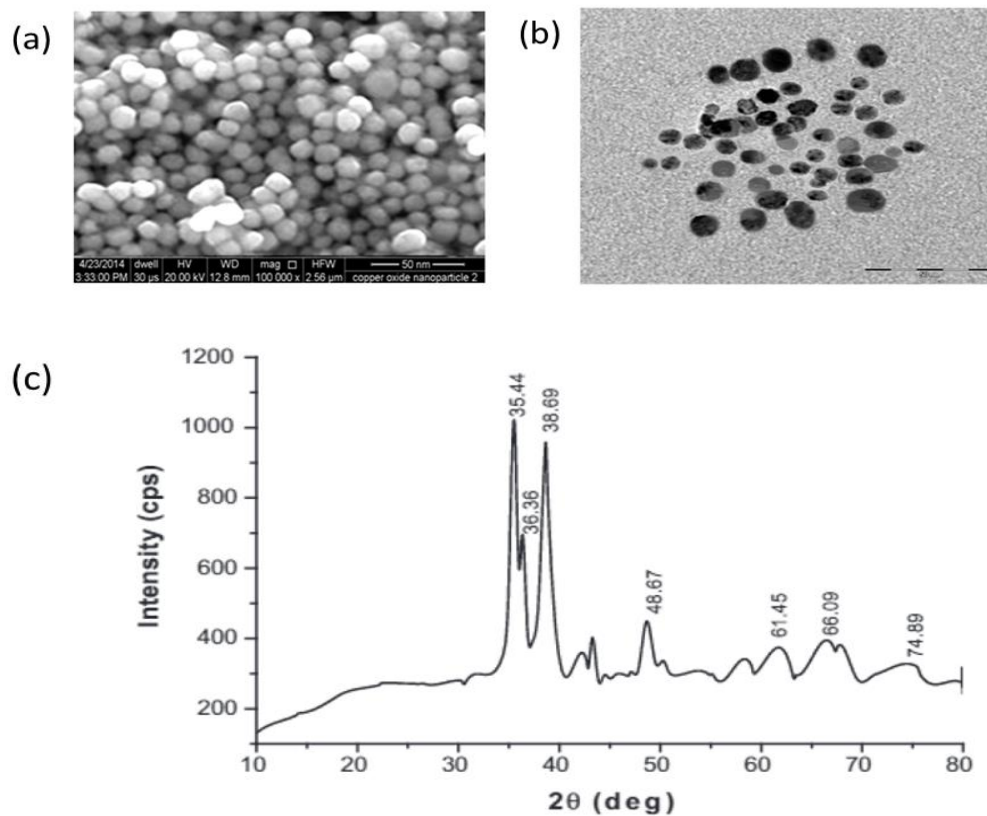
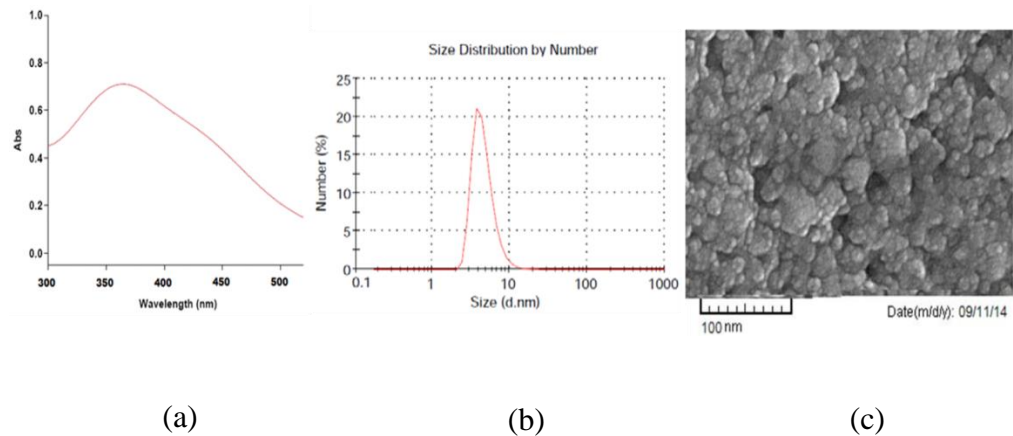


Figure 2.11: (a) SEM image, (b) TEM image and (c) XRD pattern of synthesized CuO NPs. (Mohan, et al., 2015)

2.2.3 Nanoparticles synthesis using microorganisms

The approach for green synthesis of metal oxide nanoparticles using microorganism have attract a lot of attention due to its non-toxic, environment-friendly aspects. (Chowdhury, Basu and Kundu, 2014) E.coli extracts have been utilized in biosynthesis of copper oxide nanoparticles. (Ghorbani, Fazeli and Fallahi, 2015) As the result obtained, a broad absorption peak was seen at around 365 nm which served as an evidence of formation of CuO NPs. Moreover, SEM and DLS were used to characterize the particle size of

nanoparticles. DLS illustrated the average size was approximately 5 nm meanwhile SEM analysis displayed the shape of the particles were mainly in spherical shape.



(a) (b) (c)
Figure 2.12: (a) UV-vis absorption spectra, (b) particle sizes distribution based on DLS analysis and (c) SEM image of CuO NPs using extract of E.coli. (Ghorbani, Fazeli and Fallahi, 2015)

Cuevas, et al., 2015, proposed biosynthesis of copper and copper oxide nanoparticles by *Stereum hirsutum*. The aim of this study is to investigate the capability of mycelium-free extract formed by *Stereum hirsutum* in synthesizing CuO NPs with different copper salts at different pH conditions. Synthesized CuO NPs were characterized by UV-visible spectroscopy, TEM, XRD and FT-IR. TEM result showed the nanoparticles were in all monodispersed state, spherical in shape with particle size in 4-5 nm. The XRD study confirmed the formation of Cu, Cu₂O and CuO nanocrystals. These samples display peaks at 16.5°, 22.5° and 34.6° corresponds to [110], [200] and [004] crystal patterns which is believed to be the cellulose nanofibers structure. It could be due to the presence of proteins in the fungus that lead to

formation of capped nanostructures. (Seabra and Duran, 2015) UV-visible spectroscopy showed a strong broadening peak between 590-650 nm and centred at 620 nm concluded formation of CuO NPs. In addition, the presence of proteins was further confirmed by FTIR which exhibiting few peaks at 1029 cm^{-1} , 3280 cm^{-1} and 2924 cm^{-1} assigned to C-N vibrations of aromatic and aliphatic amines, primary and secondary amines. As a result, the biosynthesis process of CuO NPs was optimum in the presence of copper chloride under neutral or alkaline condition.

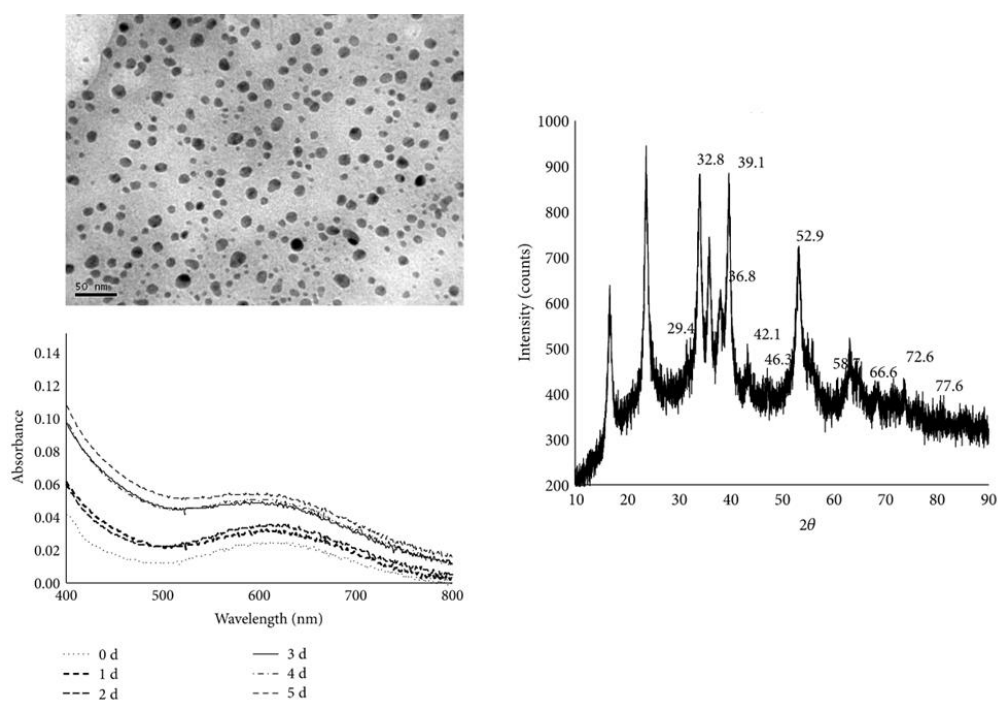


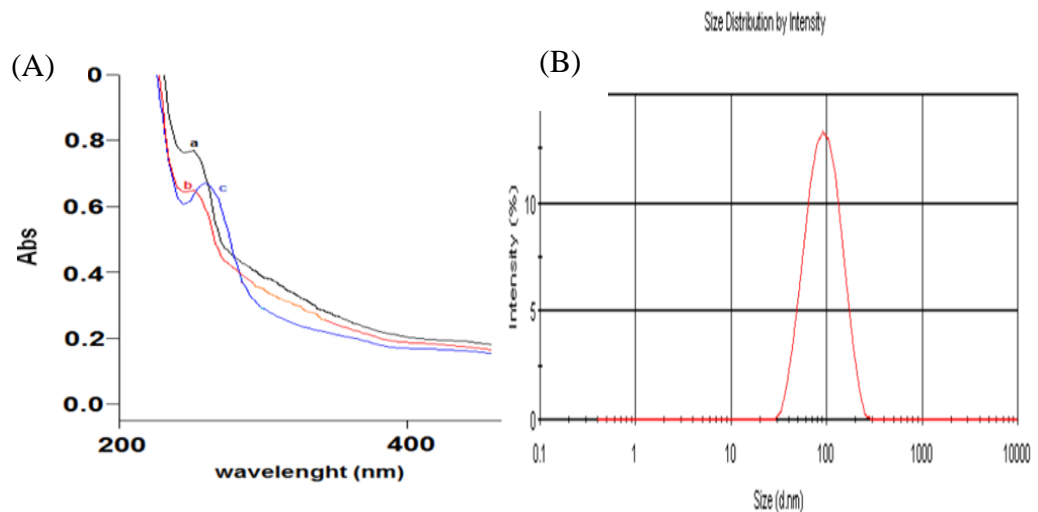
Figure 2.13: TEM image (top left), UV-Vis spectra (bottom left) and XRD pattern of synthesized CuO NPs (right). (Cuevas, et al., 2015)

As was reported by Honary, et al., 2012, they described the use of *Penicillium aurantiogriseum*, *Penicillium citrinum* and *Penicillium waksmanii* in synthesizing CuO NPs. In fact, fungi are more preferred over bacteria as a

biosource in synthesis of metal nanoparticles because they are able to secrete sufficient extracellular redox proteins in order to reduce soluble metal ions to insoluble form and form nanocrystals. (Kitching, Ramani and Marsili, 2015)

The UV-Vis spectrum recorded there is a broad absorption peak at around 265 nm indicating the electronic excitation of tryptophan and tyrosine in the protein.

SEM image provided the topographic structure and distinction of different phases in the sample. In this study, SEM image showed the nanoparticles formed were spherical shape. Besides that, DLS was used to determine the average particle size. As a result, DLS diagram revealed that the CuO NPs formed were monodispersed in well-defined dimensions. Lastly, AFM was carried out to study morphology of nanoparticles. From the topological view, it was found that the shape of nanoparticles were spherical which is correlated with the SEM result.



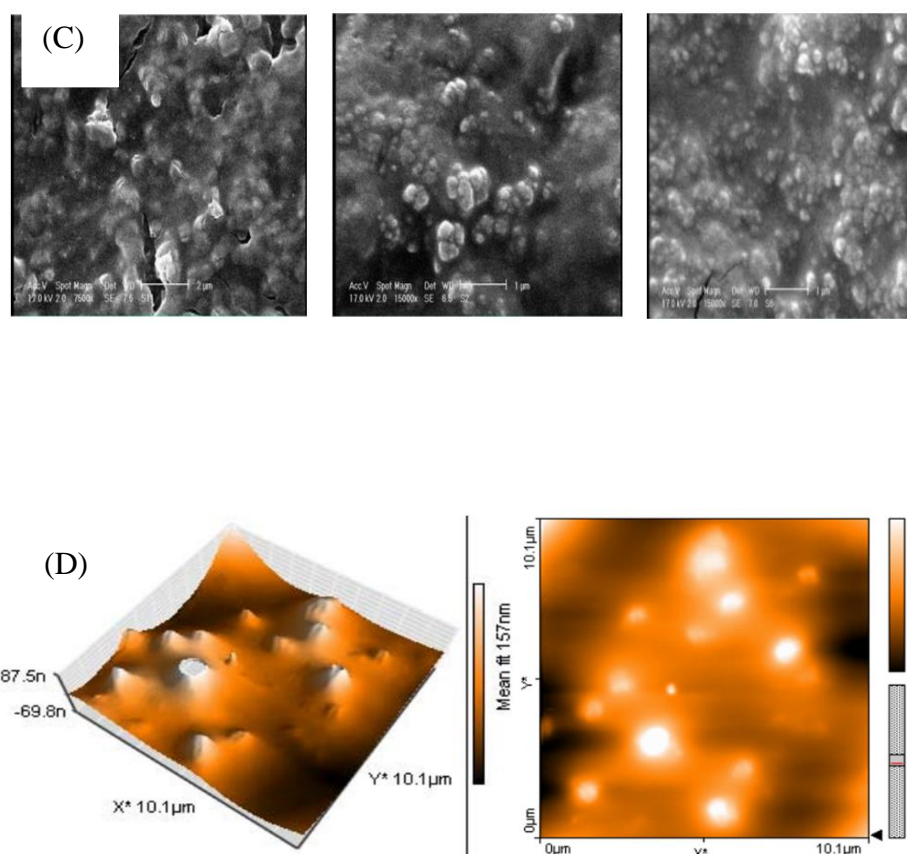


Figure 2.14: (A) UV-Vis spectra of reducing protein that presence in (a) *Penicillium citrinum*, (b) *Penicillium waksmanii* and (c) *Penicillium aurantiogriseum*. (B) DLS analysis. (C) SEM images for CuO NPs synthesis by using *Penicillium citrinum*, *Penicillium waksmanii* and *Penicillium aurantiogriseum* (from left to right). (D) AFM image of CuO NPs. (Honary, et al., 2012)

Another green approach for synthesis of CuO NPs by using *Phormidium cyanobacterium* treated with copper sulphate solution was discussed by Rahman, et al., 2009. The extracellular synthesis of CuO NPs occurs by the extracellular hydrolysis of copper initiated by metal chelating anionic proteins and reductase from cyanobacterium. (Ardelean, 2015) Biosynthesized CuO

NPs were further characterized by UV-Visible spectra displayed a characteristic peak of Cu_2O at 600 nm after 24 hours reaction time. As reaction proceeded until 36 hours, it can be seen that two adsorption peaks at ~542 nm and ~310 nm which indicates the presence of Cu_2O and CuO . A mixture of Cu_2O and CuO is produced. By the time when the reaction reached 42 hours, disappearance of 542 nm and shifting of 310 nm to 307 nm indicated the reaction of converting Cu_2O to CuO is completed. Furthermore, as XRD recorded after 42 hours, peaks at $2\theta = 35.4^\circ, 38.7^\circ, 58.3^\circ, 65.7^\circ$ and 68.0° characterized the nanoparticle sample was CuO whereas peaks at $2\theta = 48.7^\circ, 53.4^\circ, 58.3^\circ$ and 72.4° showed presence of Cu_2O . However, higher intensity peaks at 35.4° and 38.7° confirmed the sample was a mixed phase of majority CuO with small amount of Cu_2O . As TEM shown, the size of synthesized nanoparticles was 10-40 nm and some have tendency to form aggregates. SEM image illustrated the nanoparticles were distributed uniformly on protein matrix. EDX showed signals indicating presence of Cu and O while there are also weak peaks from S, C, Mg and Na. Lastly, FT-IR was performed to analyse the functional groups as a significant peak at 590 cm^{-1} assigned to Cu-O vibration stretching frequency. Another two peaks at 1650 and 1550 cm^{-1} produced by amide from protein acting as capping and stabilizing agent.

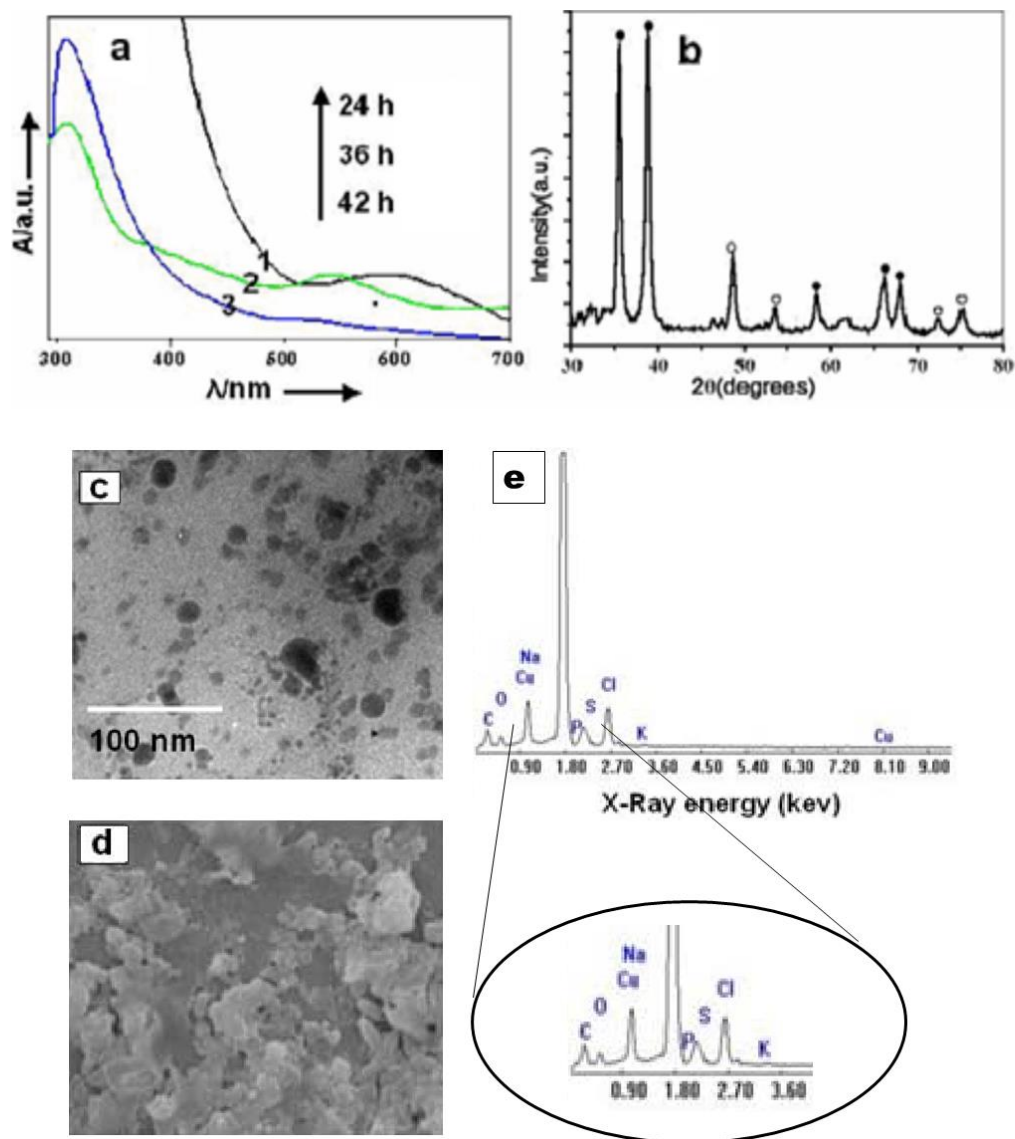


Figure 2.15: (a) UV-vis spectra synthesis reaction time of 24 h, 36h and 42 h, (b) XRD pattern, (c) TEM image, (d) SEM image of synthesized CuO NPs and (e) EDX spectrum recorded for incubated *Phormidium cyanobacterium* with copper sulphate for 42 h. (Rahman, et al., 2009)

2.3 Previous studies of CuO NPs on photocatalytic dye degradation

CuO NPs was employed as photocatalyst for dye degradation in this project. Textile and paper industries discharge huge amount of pollutants and carcinogenic dye effluents into the environment without any pre-treatment. All these dye pollutants are chemically stable which makes them hard to be degraded. Recently, photocatalytic degradation has emerged as an alternative solution to solve this problem. This is owing to its capability in decolourising and degrading the dyes to other degradation products which are not harmful to the environment.

The photocatalytic degradation of CuO NPs against Coomassie brilliant blue R-250 was studied by Sankar, et al., 2014. As a result, the maximum absorption peak was recorded 559 nm and photocatalytic degradation was achieved within 2 hours of exposure under the sunlight. The researcher highlighted the dye degradation efficiency was greatly affected by the size, morphology and surface charge property of the nanoparticles. As in accordance with the earlier findings stated that rod shaped copper oxide nanoparticles could be the more useful in degradation of coloured dye solution.

Devi and Singh, 2014 studied the photodegradation of Methyl orange (MO) by copper oxide nanoparticles synthesized from *Centella asiatica* L extract. MO solutions with the presence of CuO NPs and solution with only leaves extract were compared. As from the comparative UV-Visible spectra, there is no degradation in the absence of CuO NPs. Hence it can be concluded that

degradation of MO was initiated by the catalytic activity of CuO NPs, leaves extract does not play any role in photodegradation of dye.

Photocatalytic activity of CuO NPs was also demonstrated on Methylene blue solution (MB). (Alabi, et al., 2013) Degradation of MB was monitored by UV-Visible spectra of control solution (MB only), MB + CuO NPs and illuminated MB only. From the result obtained, only MB + CuO showed positive result. This confirmed CuO NPs possess photocatalytic activity with photodegradation efficiency of 45.12 %.

CHAPTER 3

METHODOLOGY

3.1 Chemicals

Copper nitrate trihydrate was purchased from R & M marketing, Essex, UK. Condo red and Malachite green was purchased from R & M chemicals and QRec quality reagent chemical products.

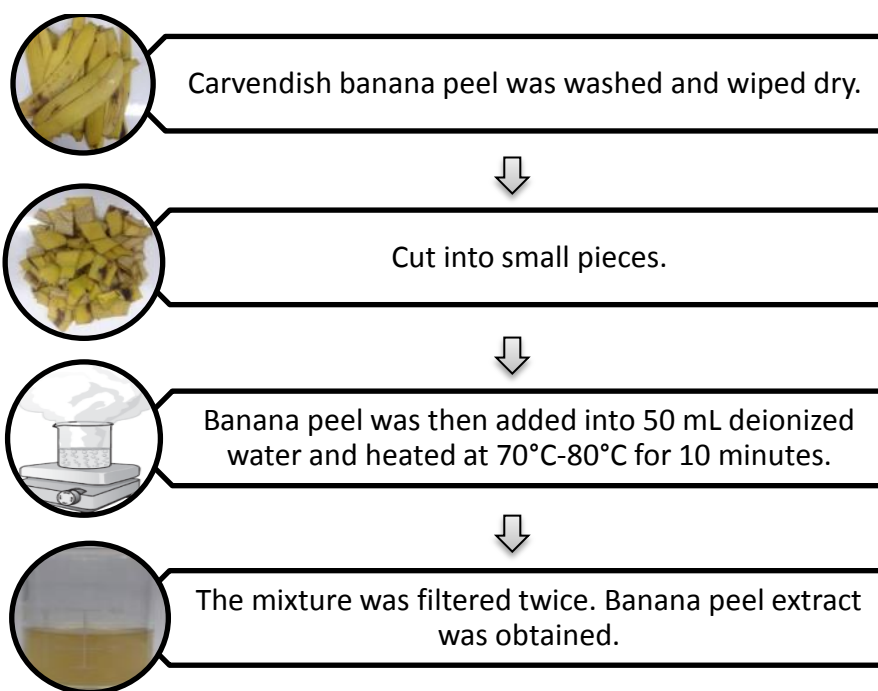
3.2 Green Synthesis of CuO NPs

3.2.1 Preparation of Cavendish banana peel extract (BPE)

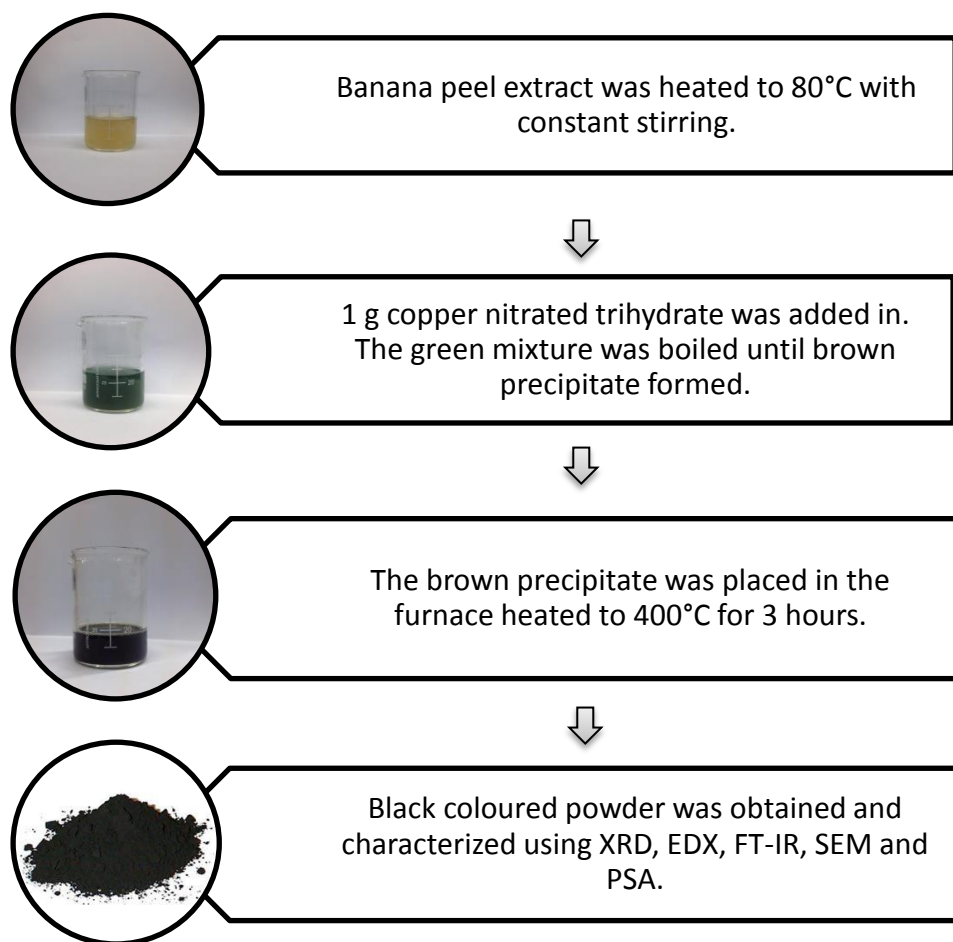
Copper oxide nanoparticles were synthesized by green synthesis method by using Cavendish banana peel as a natural source for reducing agent. The schematic diagram for synthesis process of CuO NPs was illustrated in figure 3.1. 25 g of banana peel was weighed, washed and wiped dry. After all, the banana peel was cut into pieces and added into 50 mL of deionized water. It was then heated at 70°C to 80°C for 10 minutes. The resulting extract was filtered twice and kept for further experiment.

3.2.2 Synthesis process of CuO NPs

30 mL of the banana extract was then prepared and heated at 80°C with constant stirring. 1 g of copper nitrate trihydrate was added into the hot banana peel extract. The mixture was boiled until formation of brown precipitate and then the precipitate was transferred into the crucible followed by heating in furnace at 400°C for three hours. Black coloured powder was obtained. The synthesized nanoparticles were characterized by X-ray Diffraction, Electron-dispersive X-ray spectroscopy, Fourier Transform Infrared Spectroscopy, Scanning Electron Microscopy and Particle size analyser.



(A) Preparation of banana peel extract.



(B) Synthesis and Characterization of CuO NPs.

Figure 3.1: Schematic diagram of synthesis process of CuO NPs.

3.3 Characterization of synthesized CuO NPs

The synthesized CuO NPs were characterized by using characterization techniques as follows: X-ray diffraction (XRD), Electron-dispersive X-ray spectroscopy (EDX), Fourier transform infrared spectroscopy (FT-IR), Scanning electron microscopy (SEM) and Particle size analyser. XRD was carried out by with Shimadzu XRD 6000 Cu K_{α} radiation ($\lambda = 1.5406 \text{ \AA}$, 40 kV, 30 mA, scan rate $0.02^{\circ} \text{ s}^{-1}$, scan range $30\text{-}80^{\circ}$). Elemental composition analysis was done by using Electron-dispersive X-ray spectroscopy (Oxford Instrument X-Max Energy Dispersive Diffractometer). Surface morphology of nanoparticles was examined by Scanning Electron Microscopy (JEOL JSM-6701F) operated at 3.0 kV. IR spectrum was obtained by running Perkin Elmer Spectrum RX1 Fourier Transform Infrared Spectrometer along with KBr pellet, the sample was subjected to scanning range of $4000\text{-}400 \text{ cm}^{-1}$. Particle sizes of synthesized nanoparticles were examined by Particle Size Analyser (Malvern Particle Size Mastersizer 2000).

3.4 Calculation of Crystalline size using Debye-Scherrer equation

Based on data obtained from XRD analysis, the crystalline size of nanoparticles can be calculated by using Debye-Scherrer equation as below:

$$D = \frac{k\lambda}{(\beta \cos \theta)} \quad (3.1)$$

where

D = crystalline diameter in diameter

k = Scherrer constant, 0.9

λ = wavelength of the X-ray source, (Cu K_{α} radiation = 1.5406×10^{-10} m)

β = width of diffraction broadening at full-width half maximum (in radian 2θ)

θ = angle of diffraction

β is the width of that particular diffraction peak at its full-width half maximum (FWHM) and can be determined from this formula:

$$\beta = \frac{(\text{FWHM in } 2\theta \times \pi)}{180^{\circ}} \quad (3.2)$$

3.5 Preparation of Congo red and Malachite green dye solution

A stock solution of 10 ppm dye solution was prepared by dissolving 5 mg of dye powder in 500 mL volumetric flask topped up to with distilled water. 50 mL of the dye solution was measured and poured into each of the different beakers to study the photocatalytic degradation of CuO NPs at different time intervals.

3.6 Degradation study on Congo red and Malachite green using CuO NPs as function of time

50 mg of CuO NPs was added into each of the beakers containing dye solution and allowed to stir in darkness for 30 minutes prior the commencement of the experiment. This is to maintain equilibrium between adsorption and desorption process between dye molecules and nanoparticles surface. After 30 minutes, the dye solutions with nanoparticles were placed under the exposure of sunlight irradiation. Sunlight, a source of renewable energy used as unlimited energy supply throughout the reaction. However the intensity of irradiation is not constant regards of weather conditions. Hence, the sunlight intensity was being measured at every 1 hour interval by lightmeter (Sper Scientific UVA/B lightmeter 850009). Different areas will receive sunlight at different intensities. So every replication was carried out at the same location to reduce the variable of sunlight intensity. The measured sunlight intensity was in the range of 9 – 13 mW cm⁻². At every regular time intervals, aliquot of dye sample was withdrawn and sent to centrifuge machine (Eppendorf, centrifuge 5430, operate at maximum revolutions per minutes: 7830 rpm) for centrifugation of 10 minutes. Centrifugation is to separate CuO NPs from degraded dye solution by preventing the dispersion of nanoparticles. Extra care must be taken when withdrawing the sample from centrifuge tube as to avoid disturbing the deposition of nanoparticles on the wall of centrifuge tube. A slight move can cause resuspension of nanoparticles in dye solution. By doing this, a clean supernatant solution can be obtained, make sure there is no traces of nanoparticles in the sample which could leads to inaccurate result. Presence of

nanoparticles can contribute to amount of light scattering during the absorbance measurement. The result will be biased as the measurement is not due to the light absorbed by dye sample alone anymore. After centrifugation, the sample was subjected to UV-Vis Single Beam Spectrophotometer (Thermo Fischer Scientific Genesys 10S series UV-Visible spectrophotometer) scanning in the range of 200 to 800 nm. The maximum wavelength of Congo red and Malachite green was recorded as 495 nm and 618 nm respectively.

3.7 Determination of degradation percentage

Degradation percentage of dye solution was calculated by taking the absorbance values recorded at λ_{\max} before and after photocatalytic degradation.

The equation was provided as shown:

$$\text{Degradation percentage} = \frac{A_0 - A_t}{A_0} \times 100 \% \quad (3.3)$$

where

A_0 = initial absorbance of dye solution before expose to sunlight

A_t = absorbance of dye solution at different time intervals, t

CHAPTER 4

RESULTS AND DISCUSSION

4.1 Synthesis of CuO nanoparticles

In this study, natural synthesis of CuO NPs was successfully accomplished by using Cavendish banana peel extract (BPE) as a green synthesizer. Banana peel is the major food waste in pulp industry and it was known to contain abundance of bioactive compounds like polyphenols, carotenoids which exhibiting biological effects such as antioxidant, anti-carcinogenic and anti-mutagenic. (Sundaram, et al., 2011) In this case, BPE can be used as a reducing and capping agent. (Ibrahim, 2015) This greener approach was exploited as it is easier to be carried out without any complicated experimental procedure. In addition, this method is comparatively low cost as the natural agricultural waste (banana peel) has been utilized as the synthesizer and free of solvents. The CuO NPs was synthesized by reaction between BPE and copper nitrate trihydrate. BPE used to reduce the copper ions (Cu^{2+} to Cu^0). Reduction process can be confirmed by the development of colour change from blue to green colour solution and slowly into brown precipitate.



Figure 4.1: Synthesized CuO NPs.

Copper nitrate trihydrate was used as a source for copper in this experiment.

The synthesis process is as follow:

- I. BPE that prepared from the previous experiment was heated until it reaches 80°C . The temperature of BPE must be controlled from increasing beyond 100°C as organic compounds that present inside banana peel can be decomposed at such a high temperature. After all copper nitrate trihydrate was then added slowly into the hot BPE with magnetic stirring to form green solution. Formation of precipitate as a result of heating copper nitrate trihydrate.

- II. Upon continuous heating, the green solution slowly turned into darker green coloured solution with formation of brown precipitate. It was suggested that reduction process of copper salt, Cu(II) to copper (Cu) can be confirmed by adding chemical reducing agent into the copper nitrate trihydrate alone. In the case of same colour change was observed, it can be said that reduction has been taken place. Upon calcination, copper oxide is formed.

Synthesized CuO NPs were then further drying in an oven to remove the excess water molecules present in CuO NPs.

4.2 Characterization of CuO NPs

After CuO NPs was being synthesized, the black coloured powder was obtained as showed in figure 4.1. CuO NPs were characterized by X-Ray Diffraction (XRD), Energy-dispersive X-Ray Spectroscopy (EDX), Fourier Transform Infrared Spectroscopy (FT-IR), Scanning Electron Microscopy (SEM) and particle size analyser (PSA).

4.2.1 X-Ray Diffraction

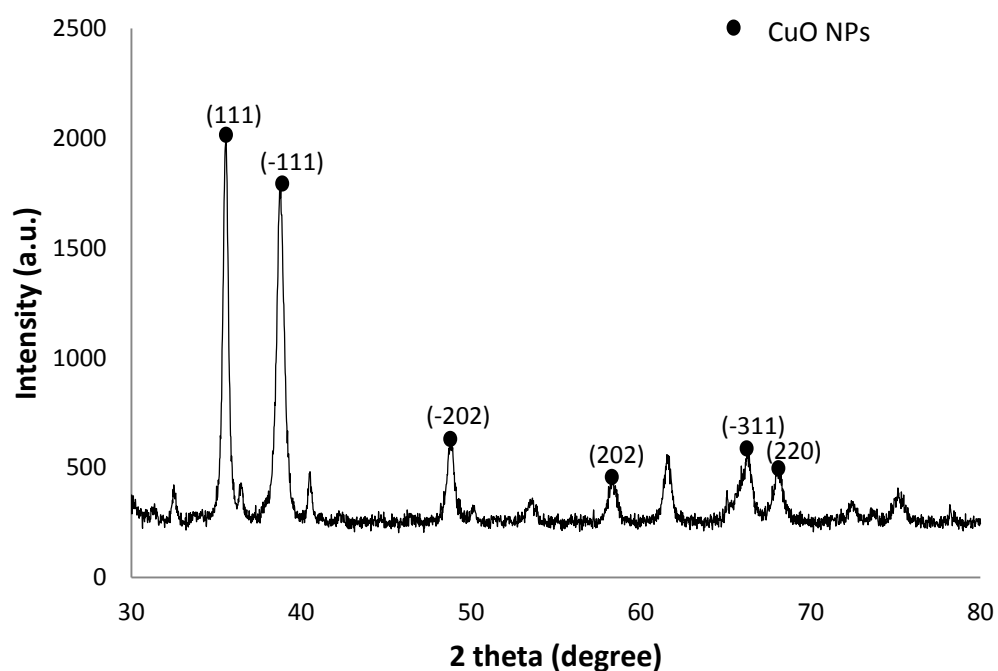


Figure 4.2: XRD pattern of synthesized CuO NPs.

Figure 4.2 shown the XRD pattern of synthesized CuO NPs. XRD pattern displayed that most of the diffraction peaks at 2θ values 35.52° , 38.75° , 48.76° , 58.29° , 66.30° , 68.02° were assigned to (111), (-111), (-202), (202), (-311) and (220) crystal planes. Similar result was obtained by Wu, et al., 2010. The XRD patterns of synthesized CuO NPs were closely matched with the

standard data JCPDS card no. 48-1548 that suggesting a monoclinic (tenorite) phase crystalline structure. (Rao and Venkatarangaiah., 2014) Broadening of the peaks in diffractogram demonstrated that the nanoparticle synthesized was a nanostructure with low crystallinity of 16.1844%. The file was attached in Appendix A. The crystalline size of the CuO NPs was calculated using Debye Scherrer equation. As a result, the crystalline size of CuO NPs corresponds to the highest peak was calculated to be 22.60 nm. The calculation was shown in Appendix B.

4.2.2 Energy-dispersive X-Ray Spectroscopy

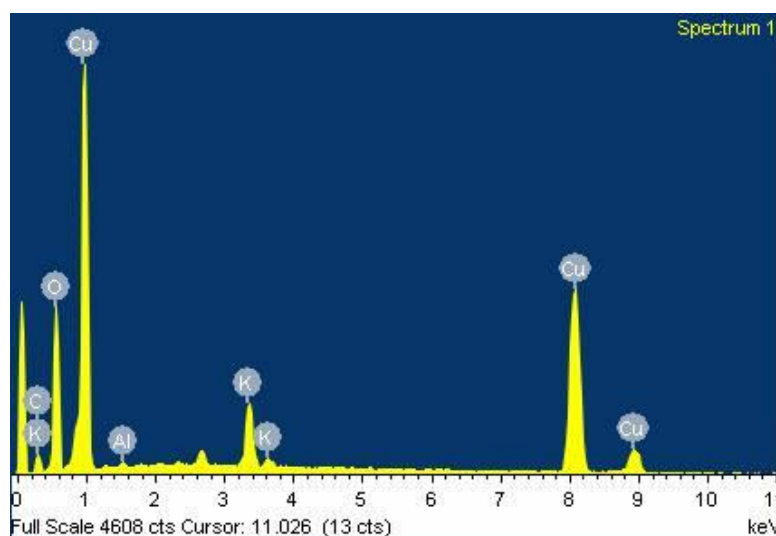


Figure 4.3: EDX spectrum of CuO NPs.

EDX result revealed that the sample contains elements of copper and oxygen confirmed the formation of CuO NPs. The weight percents of copper, oxygen, aluminium, potassium and carbon were found out to be 60.38 %, 26.75 %, 0.56 %, 3.90 % and 8.41 % respectively. Traces of aluminium were due to the contaminants from the chemicals, a slight amount of potassium came from

banana peel extract. Lastly, carbon was attributed by the phenolic compounds (biomolecules) that present in the banana peel extract which surrounded on the nanoparticles surface. Repeated washing with distilled water and absolute ethanol can be done to eliminate the traces of carbon and potassium in order to obtain a pure sample.

4.2.3 Fourier Transform Infrared Spectroscopy

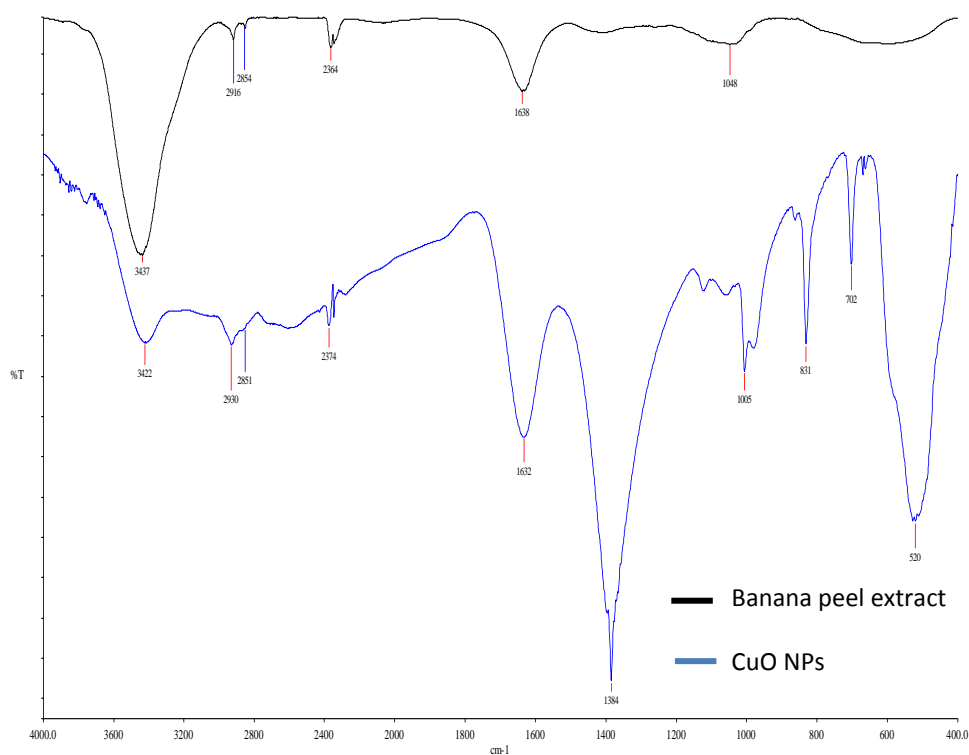


Figure 4.4: FT-IR comparative spectrum of synthesized CuO NPs and BPE.

FT-IR measurement was performed to identify the possible significant functional groups that responsible for reducing and capping CuO NPs. Furthermore, FTIR spectra also can be used to identify the characteristics peak of Cu-O bonding. Based on the FTIR spectrum of CuO NPs, the most significant absorption peak at 520 cm⁻¹ was assigned to Cu-O bond confirmed

the formation of CuO NPs. There is a study reported that CuO (M-O) stretching occurs at 528 cm^{-1} . (Sundaramurthy and Parthiban., 2015) This was supported by another strong intensity peak at 1384 cm^{-1} indicates the presence of $\text{Cu}^{2+}\text{-O}^{2-}$ stretching mode which in accordance with the finding by (Li, 2008). There is no other absorption peak at $700\text{ -}500\text{ cm}^{-1}$ possibly attributed to Cu(I)-O vibration ($\sim 623\text{ cm}^{-1}$) in the spectrum which excluded the presence of any Cu_2O nanoparticles. (Kooti and Matouri., 2010) A weak broad peak at 3422 cm^{-1} was corresponds to the O-H stretch (H-bonded alcohols) due to the presence of absorbed water molecules. Nanoparticles are capable in absorbing moisture from surrounding by having high surface area to volume ratio. (Luna, et al., 2015; Shyla, 2015) Absorption peaks at 2930 cm^{-1} and 2851 cm^{-1} were attributed to asymmetric and symmetric C-H stretching mode which caused by the phenolic compounds. C=O vibration produced a peak at 1632 cm^{-1} from the carboxylic acid group whereas specific peak at 2374 cm^{-1} represents NH^+ stretching in charged amines ($\text{C}=\text{NH}^+$). Shifting of these following peaks were observed in IR spectrum of CuO NPs such as 3437 to 3422 , 2920 to 2030 , 2364 to 2374 and 1638 to 1632 indicates that carboxyl, hydroxyl group in banana peel extract was taking part in the synthesis of CuO NPs. It was suggested that carbonyl and hydroxyl group are strongly attracted towards the copper oxide thus surrounded on surface of nanoparticles in order to stabilize the nanoparticles and prevent agglomeration. (Ganapuram, et al., 2015)

In IR spectrum of CuO NPs, an adsorption peak at 831 cm^{-1} was attributed to NH_2 amine group followed by another peak at 702 cm^{-1} resulted from C-H bending out of plane. However, these peaks correspond to the functional

groups of biomolecules from banana peel were found to be absent in IR spectrum of banana peel extract. Some peaks missed out from IR spectrum of banana peel extract due to inappropriate preparation method of extracting active compounds from banana peel.

4.2.4 Scanning Electron Microscopy

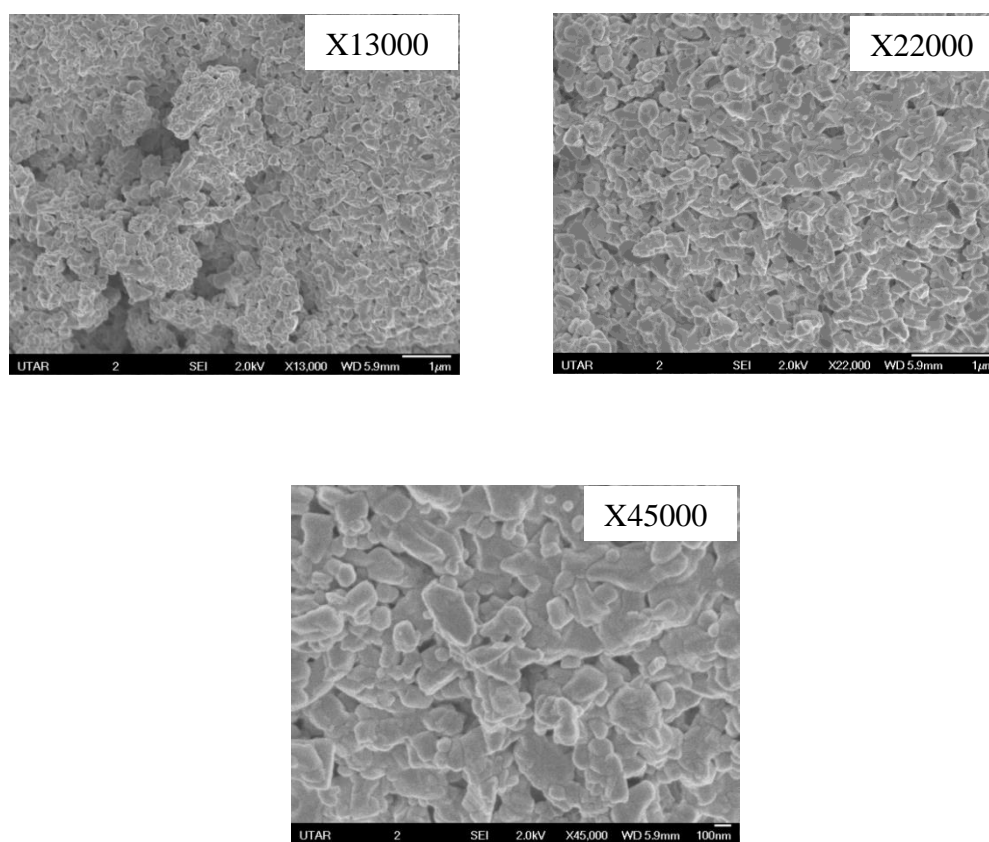
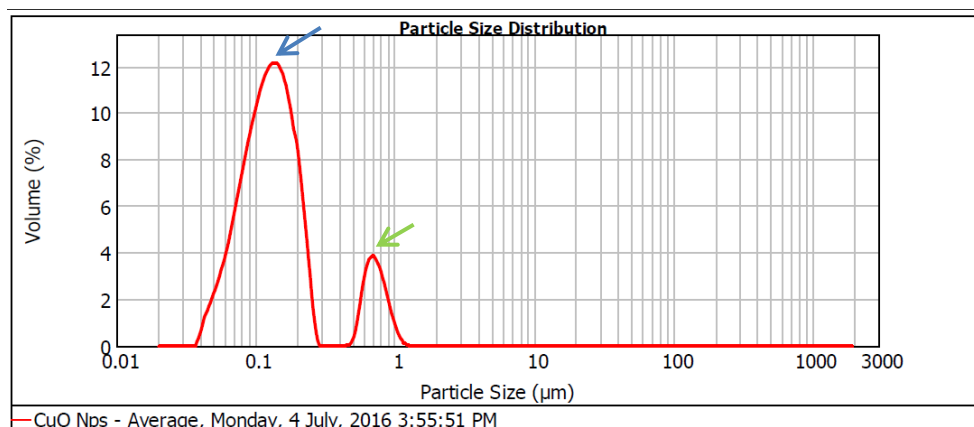


Figure 4.5: SEM images of CuO NPs with different magnifications $X = 13000$, 22000 and 45000 .

From the SEM image, it can be seen that the majority of the nanoparticles are in irregular and dumbbell shape. Many of the nanoparticles were exist in highly agglomerated form. As a result, the average particle sizes of CuO NPs were found out to be 91.0 nm .

4.2.5 Particle Size Analyser



Size (µm)	Volume In %										
0.010	0.00	0.105	10.10	1.096	0.10	11.482	0.00	120.226	0.00	1258.925	0.00
0.011	0.00	0.120	10.86	1.259	0.00	13.183	0.00	138.038	0.00	1445.440	0.00
0.013	0.00	0.138	10.89	1.445	0.00	15.136	0.00	158.489	0.00	1659.587	0.00
0.015	0.00	0.158	9.97	1.660	0.00	17.378	0.00	181.970	0.00	1905.461	0.00
0.017	0.00	0.182	8.00	1.905	0.00	19.953	0.00	208.930	0.00	2187.762	0.00
0.020	0.00	0.209	5.00	2.188	0.00	22.909	0.00	239.883	0.00	2511.886	0.00
0.023	0.00	0.240	1.47	2.512	0.00	26.303	0.00	275.423	0.00	2884.032	0.00
0.026	0.00	0.275	0.00	2.884	0.00	30.200	0.00	316.228	0.00	3311.311	0.00
0.030	0.00	0.316	0.00	3.311	0.00	34.674	0.00	363.078	0.00	3801.894	0.00
0.035	0.00	0.363	0.00	3.802	0.00	39.811	0.00	416.869	0.00	4365.158	0.00
0.040	1.06	0.417	0.00	4.385	0.00	45.709	0.00	478.630	0.00	5011.872	0.00
0.046	1.86	0.479	0.39	5.012	0.00	52.481	0.00	549.541	0.00	5754.399	0.00
0.052	2.84	0.550	2.31	5.754	0.00	60.256	0.00	630.957	0.00	6606.934	0.00
0.060	4.06	0.631	3.43	6.607	0.00	69.183	0.00	724.436	0.00	7585.776	0.00
0.069	5.70	0.724	3.09	7.586	0.00	79.433	0.00	831.764	0.00	8709.636	0.00
0.079	7.35	0.832	1.91	8.710	0.00	91.201	0.00	954.993	0.00	10000.000	0.00
0.091	8.87	0.955	0.73	10.000	0.00	104.713	0.00	1096.478	0.00		
0.105		1.096		11.482		120.226		1258.925			

Figure 4.6: Size distribution histogram of CuO NPs.

Table 4.1: Crystalline sizes and average particle sizes of CuO NPs.

Sample	Crystalline size, XRD (nm)	Particle size, PSA (nm)
CuO NPs	22.60	120-138

Particle size distribution histogram above revealed that the most intense peak (indicated by blue arrow) whose centred at 120-138 nm tells that majority of the particle sizes lie within this range with only small amount of them (indicated by green arrow) having a larger particle size of 631-724 nm as a result of agglomeration. This is agreed with the SEM images showing particles clumped together to form larger particles.

4.3 Degradation of dye solution by CuO NPs

In this study, degradation of Congo red and Malachite green dye solution were performed to study photocatalytic activity of CuO NPs. UV-Vis Single Beam Spectrophotometer was used in this research study to measure the absorbance of dye solution before degradation and after degradation at time, t of exposure under sunlight radiation.

4.3.1 Congo red dye degradation under solar irradiation

Figure 4.8 showed the UV-Vis spectra of dye degradation of Congo red solution by CuO NPs as a function of contact time. At different time intervals, the absorbance measurements of Congo red solution was recorded at $\lambda_{\max} = 495$ nm. The λ_{\max} of Congo red was found closely matched with the λ_{\max} of 505 nm reported by (Guo, et al., 2013).

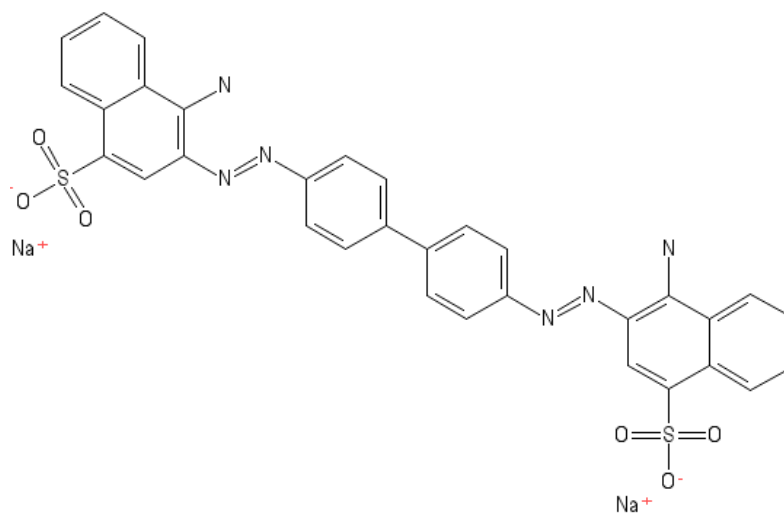


Figure 4.7: Molecular structure of Congo Red. (Shu, et al., 2015)

Based on the spectra, it was clearly seen that the intensity of absorption peak at λ_{\max} decreases as reaction time increases from 0 minutes to 150 minutes. The absorbance depends on the number of molecules reacted with it. In other words, the highest adsorption peak of degraded dye contains highest concentration of Congo red dye solution yet to be degraded. From the UV-Vis spectra, the wavelength range was measured at the range between 200 to 800 nm. Two adsorption peaks were observed, one of the peaks was seen at 345 nm and the other one at 495 nm which corresponds to a study by (Ganapuram, et al., 2015) claiming that Congo red showed adsorption at 498 nm ($\pi \rightarrow \pi^*$) and 350 nm ($n \rightarrow \pi^*$).

New peak was appeared at around 370 nm which served as an evident for the destruction of Congo red dye molecules through the photodegradation. Decolourization was attributed to biodegradation with two outcomes either the peak corresponds to the maximum wavelength completely flattened or being shifted to another wavelength giving rise to generation of new peak in the

spectrum. (Babu, et al., 2015) Formation of new peak was due to the different intermediate metabolites formed during degradation (decolourization) of Congo red. However, the degraded products that give rise to this new peak cannot be defined exactly as the degradation mechanism of Congo red upon solar irradiation has not been devised.

It was observed that a large gap appeared in between the control and the first time interval, the degradation efficiency was shooting up to 47.21 % at the first 15 minutes. The rapid removal of dye solution at the initial adsorption stage leading to a drastic decrement in absorbance reflects the adsorption capability of dye molecules to the nanoparticles surface. (Movahedi, et al., 2009) After the adding of CuO NPs, the solution was stirred for 30 minutes and reached equilibrium between adsorption and desorption. The dye molecules were allowed to adsorb on the surface active sites where adsorption occurs through two oxygen atoms of sulphonate group of Congo red with CuO particles surface. As time increases, the surface active sites of CuO NPs was gradually occupied by dye molecules and reached a saturation point. Consequently, less number of surface active sites were be available for further adsorption then followed by photodegradation which was a relatively slow process. This explained why there is only a slight increase in degradation percentage over contact time up to 150 minutes. From the calculation, the highest degradation percentage achieved by CuO NPs on Congo red was 88.83 %. Furthermore, the dye degradation can also be visually detected by the gradual colour change from red to almost colourless as shown in Figure 4.9.

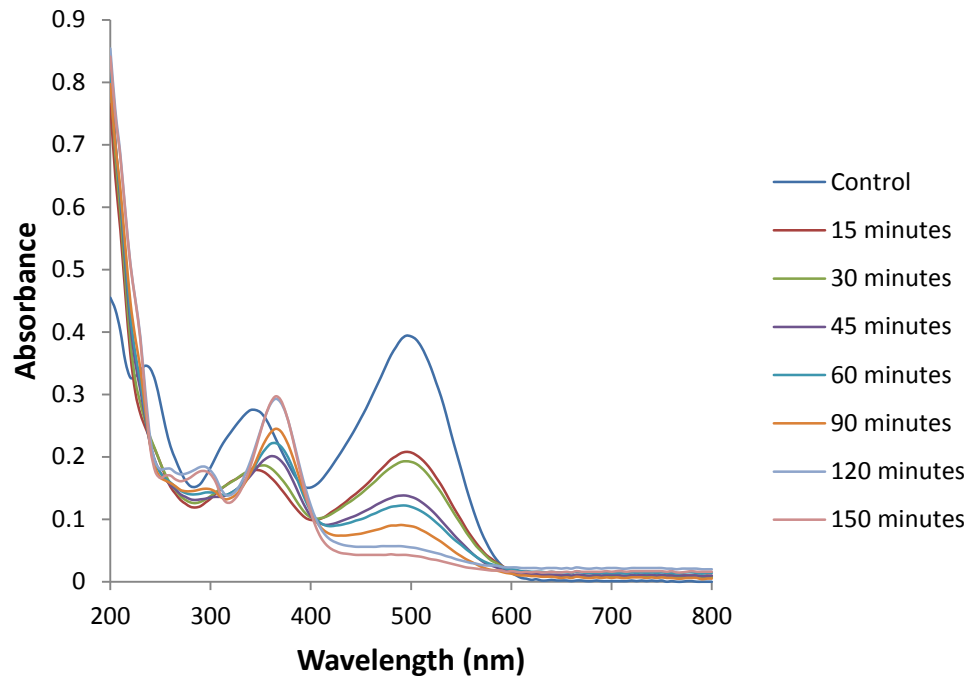


Figure 4.8: UV-Vis spectra of Congo red dye degradation as a function of time.

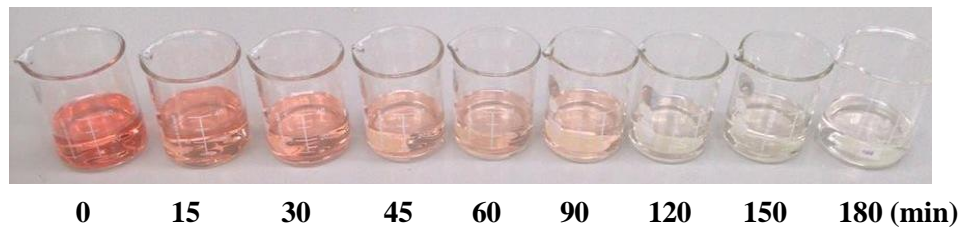


Figure 4.9: Decolourization of Congo red solution at different time intervals.

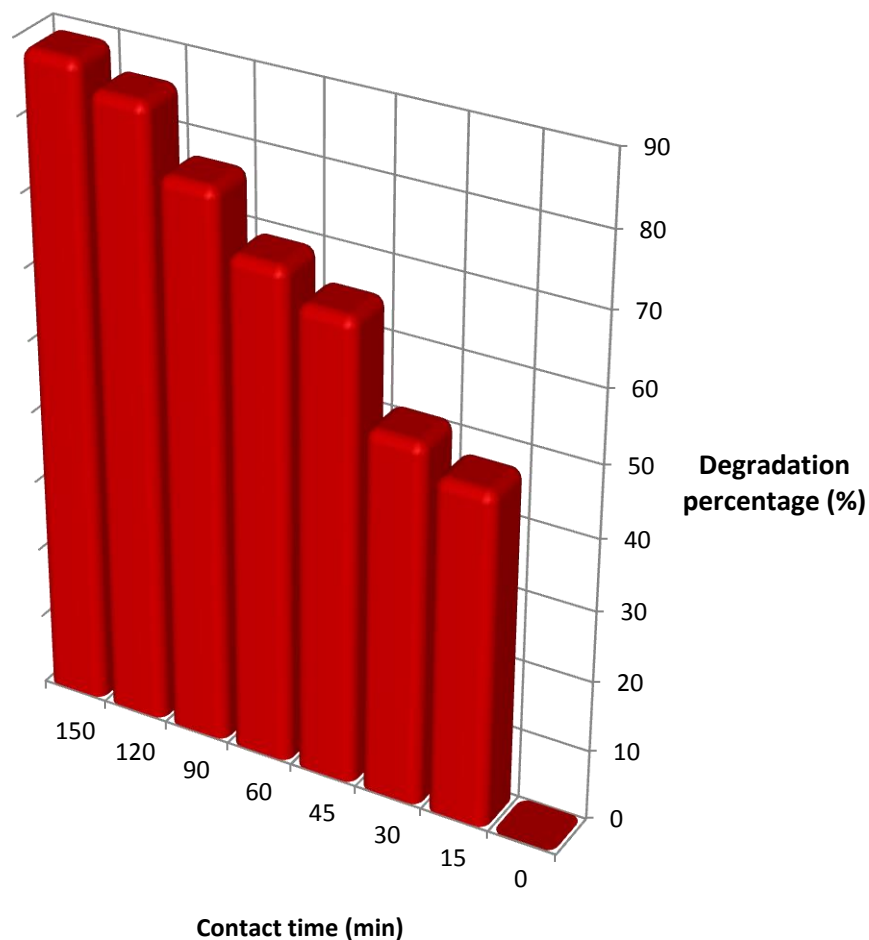


Figure 4.10: Degradation percentage of Congo red at different time intervals.

4.3.2 Malachite green dye degradation under solar irradiation

In this study, degradation of Malachite green by CuO NPs was also investigated. Aliquot of each of the sample will be taken at different time intervals and the absorbance of the samples were measured spectrophotometrically at $\lambda_{\text{max}} = 618 \text{ nm}$ which similar to study done by (Ameta, et al., 2014) which reported maximum wavelength of 620 nm.

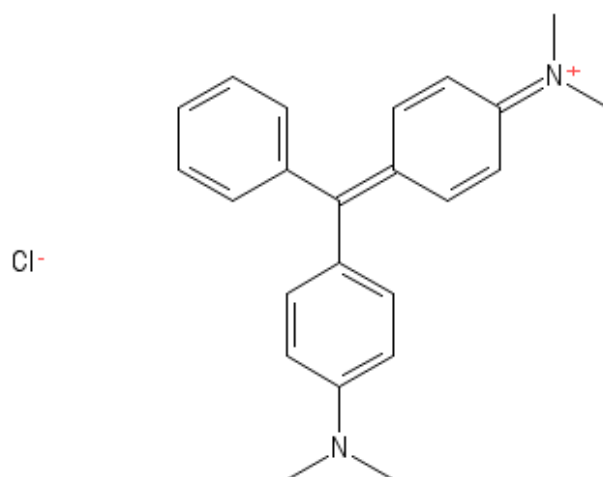


Figure 4.11: Molecular structure of Malachite green. (Kumawat, et al., 2015)

It was observed that the absorbance of dye solution decreases against time. Thereafter, the concentration of dye solution decreases as reaction time increases. This can be clearly indicated by the decolouration of Malachite green from greenish-blue to almost colourless solution. The UV-Vis spectra of Malachite green dye degradation showed the similar trend as what we obtained for Congo red dye solution. The intensity of adsorption peaks at 618 nm decrease with increasing irradiation time. At the beginning of the reaction, dye degraded tremendously as compared with the degradation rate for the subsequently time intervals thereby the rate of degradation was seen to be very slow after the first 10 minutes. The degradation at the initial stage was very rapid but no hypsochromic shift was seen in this spectrum. This demonstrated that photodegradation mechanism of cleavage at the whole conjugated chromophore group of Malachite green structure was more favoured. (Chen, et al., 2006) In addition, the other two peaks centred at ~ 420 nm and ~ 310 nm slowly decrease as well. At the same time, it can be observed that a new peak arisen at around 350 nm over time. This can be explained by random

decomposition of Malachite green in many ways as destruction of polyaromatic rings or formation of intermediate products without conjugated system can give rise to the appearance of this new peak. (Afshar et al., 2011)

There is another possible mechanism which happened during the irradiation. Malachite green dye molecules absorbed energy and formed excited singlet state underwent intersystem crossing (ISC) to triplet state. Malachite green was then converted into its leuco form upon being reduced by superoxide anion radical (O_2^-) resulted from abstraction of excited electron by oxygen molecule. Eventually leuco form of Malachite green will degrade to other degradation products. Figure 4.12 shows the tentative photocatalytic mechanism of Malachite green.

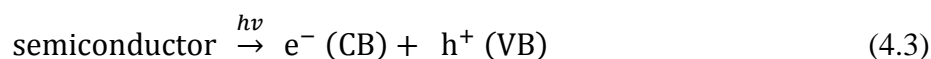
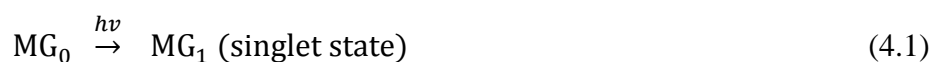


Figure 4.12: Tentative photocatalytic mechanism of Malachite green. (Ameta, Papnai and Ameta, 2014)

The degradation effect on Malachite green was not that prominent after the first 10 minutes exposure to sunlight. At the beginning stage, adsorption is more likely to happen (rapid process). Thereafter, dye degraded in slow rate after adsorption throughout the whole photodegradation process. This is

because the surface active sites of CuO NPs were already being occupied by previous dye molecules hence the number of available, free surface active sites of nanoparticles for the subsequent adsorption will be greatly reduced. This will indirectly influence the rate of degradation because adsorption must be happened first then followed by degradation of the dye molecules. In this case, the highest degradation percentage achieved was 91.78 % and the decolourization of Malachite green can be seen at Figure 4.14.

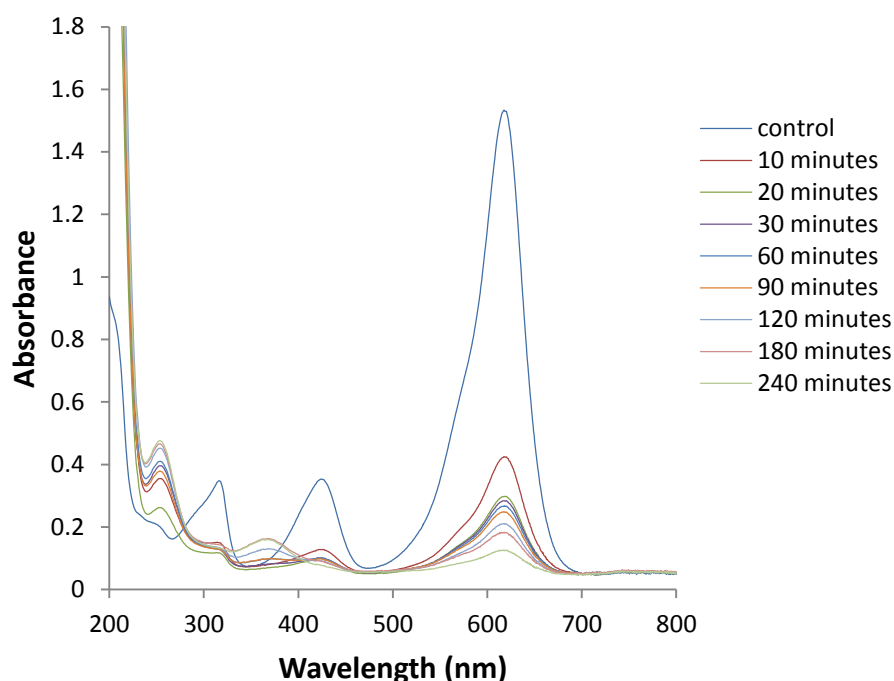


Figure 4.13: UV-Vis spectra of Malachite green dye degradation as a function of time.

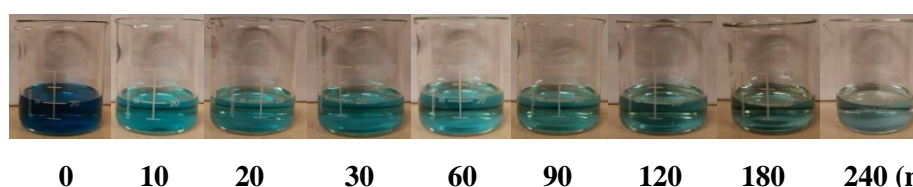


Figure 4.14: Decolourization of Malachite green solution at different time intervals.



Figure 4.15: Malachite green dye solution before and after degradation.

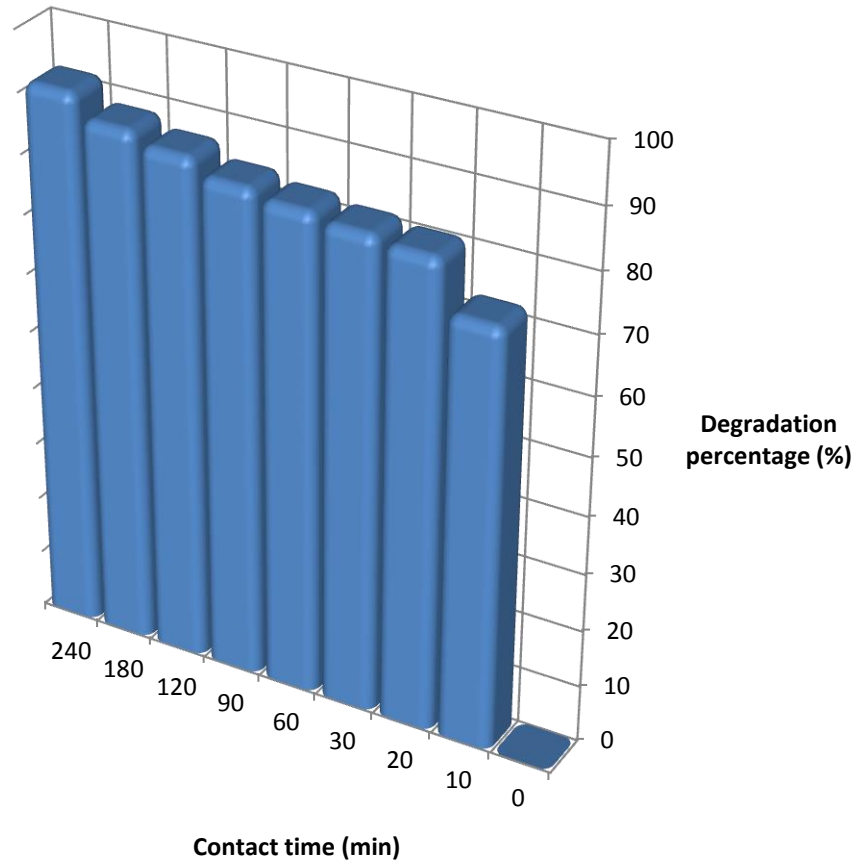


Figure 4.16: Degradation percentage of Malachite green at different time intervals.

4.3.3 Degradation comparison of Congo red and Malachite green dye solution

Photocatalytic activity of CuO NPS on Congo red and Malachite green dye solution were evaluated. On the contrary, degradation efficiency of Congo red and Malachite green were found to be 88.83 % and 91.78 % respectively. On the other hand, the degradation efficiencies at the 120 mins were 85.53 % for Congo red and 86.24 % for Malachite green. It was observed that the degradation of Malachite green was higher as compared to Congo red. It showed that photocatalytic degradation not merely on destruction of conjugate system only but also the intermediate products. (Katwal, et al., 2015) Based on the structure itself, Malachite green was found out to be more susceptible to oxidation where Congo red is more stable due to the presence of biphenyl group and naphthenic group providing large steric hindrance effect. Effect of contact time on degradation (decolouration) of dye was illustrated in Figure 4.8 and 4.13 for Congo red and Malachite green solution. It can be seen that dye degradation increases over time exposure. As mentioned earlier, both dye showed rapid initial degradation which is due to interaction of nanoparticle surface and dye molecules. As a result, this interaction happened to be faster than solute-solute interactions. (Roy and Mondal, 2014)

CHAPTER 5

CONCLUSION

In this study, CuO NPs was successfully synthesized by green synthetic pathway. Cavendish banana peel was utilized as a natural reducing and capping agent in synthesizing CuO NPs. The identification of CuO NPs was done by characterization techniques such as XRD, EDX, FT-IR, SEM and PSA. XRD diffractogram confirmed the sample was CuO NPs with crystalline size of 22.60 nm. Synthesized CuO NPs is a nanostructure with low crystallinity of 16.1844 % only. Furthermore, SEM image revealed the average particle size was 91.0 nm and exist in dumbbell and irregular shape of highly agglomerated form.

Besides, CuO NPs has been proven to be possessing excellent photocatalytic activity. Photocatalytic degradation effect exerted on Congo red and Malachite green was a great success as it showed degradation efficiency of 88.83 % and 91.78 % respectively. Consequently, the longer the time exposure, the better the photocatalytic degradation on dye tested. In most cases, absorbance measurement of first dye sample was a rapid drop as photocatalytic degradation occurs in two pathways: (i) adsorption of dye molecules onto surface of nanoparticles, (ii) degradation of dye molecules by CuO NPs. Adsorption will be taken place prior expose to sunlight whereby adsorption is

relatively fast process hence leading to the sudden decrease in absorbance at initial stage of dye degradation. On the other hand, the free surface actives of nanoparticles will be getting exhausted over reaction time as more and more of them being occupied by dye molecules. Therefore, the degradation rate becomes slower at the subsequent time intervals.

Application of CuO NPs as a photocatalyst in degrading the commercial dye in wastewater treatment can be included in future study. Depth of the wastewater (sunlight penetration), sunlight intensity and reusability of CuO NPs have to be taken into consideration as all these factors could affect the degradation effect of CuO NPs exerted on the commercial dye. Furthermore, it was suggested to carry out GC-MS and LC-MS to determine the intermediate products formed during dye degradation thus propose a tentative mechanism through the fragmentation pathway.

REFERENCES

Journals

- Abboud, Y., Saffaj, T., Chagraoui, A., El Bouri, A., Brouzi, K., Tanane, O. and Ihssane, B., 2014. Biosynthesis, characterization and antimicrobial activity of copper oxide nanoparticles (CONPs) produced using brown alga extract (*Bifurcaria bifurcata*). *Applied Nanoscience*, pp. 571-576.
- Afshar, S., Jahromi, S. H., Jafari, N., Ahmadi, Z. and Hakamizadeh, M., 2011. Degradation of malachite green oxalate by UV and visible lights irradiation using Pt/TiO₂/SiO₂ nanophotocatalyst. *Scientia Iranica Transactions F: Nanotechnology*, 18(3), pp. 772-779.
- Agnihotri, M., Joshi, A., Kumar, R., Zinjarde, S. and Kulkarni, S., 2009. Biosynthesis of gold nanoparticles by the tropical marine yeast *Yarrowia lipolytica* NCIM 3589. *Materials letters*, 63(15), pp. 1231-1234.
- Ahmad, A., Senapati, S., Khan, M. I., Kumar, R., Ramani, R., Srinivas, V. and Sastry, M., 2003. Intracellular synthesis of gold nanoparticles by a novel alkalotolerant actinomycete, *Rhodococcus* species. *Nanotechnology*, 14(7), pp. 824-828.
- Akthar, M. S., Birhanu, G. and Demisse, S., 2014. Antimicrobial activity of *Piper nigrum* L. and *Cassia didymobotyra* L. leaf extract on selected food borne pathogens. *Asian Pacific Journal of Tropical Disease*, 4(2), pp. 911-919.
- Alabi, A. B., Coppede, N., Vilani, M., Calestani, D., Zappetini, A., Babalola, O. A. and Salvatore, I., 2013. Photocatalytic activity of nanostructured copper(II) oxide particles. *Ife Journal of Science*, 15(2), pp. 409-414.
- Ameta, K., Tak, P., Soni, D. and Ameta, S. C., 2014. Photocatalytic decomposition of malachite green over lead chromate powder. *Scientific Reviews & Chemical Communications*, 4(1), pp. 38-45.

- Ameta, K. L., Papnai, N. and Ameta, R., 2014. Photocatalytic degradation of Malachite green using nano-sized cerium-iron oxide. *Orbital: The Electronic Journal of Chemistry*, 6(1), pp. 14-19.
- Ang, W., Xiong, L., Sun, L., Liu, Y. J. and Li, W. W., 2013. CuO nanoparticles modified ZnO nanorods with improved photocatalytic activity. *Chinese Physics Letters*, 30(4).
- Armendariz, V., Gardea-Torresdey, J. L., Herrera, I., Jose-Yacaman, M., Peralta-Videa, J. R. and Santiago, P., 2004. Size controlled gold nanoparticles formation by *Avena sativa* biomass: use of plants in nanobiotechnology. *Journal of Nanoparticles Research*, 6(4), pp. 377-382.
- Babu, S. S., Mohandass, C., Vijayaraj, A. S. and Dhale, M. A., 2015. Detoxification and color removal of Congo red by a novel *Dietzia* sp. (DTS26)-A microcosm approach. *Ecotoxicol Environmental Safety*, vol 114, pp. 52-60.
- Baker, S., Rakshith, D., Kavitha, K. S., Santosh, P., Kavitha, H. U., Rao, Y. and Satish, S., 2013. Plants: Emerging as nanoparticles towards facile route in synthesis of nanoparticles. *BioImpacts*, 3(3), pp. 111-117.
- Chandran, S. P., Ahmad, A., Chaudhary, M., Pasricha, R. and Sastry, M., 2006. Synthesis of gold nanoparticles and silver nanoparticles using *Aloe vera* plant extract. *Biotechnology Progress*, 22(2), pp. 577-583.
- Chatterjee, S., Chatterjee, S., Dey, K. and Dutta, S., 2013. Study of antioxidant activity and immune stimulating potency of the ethnomedicinal plant, *Cassia alata* (L.) Roxb. *Medicinal Aromatic Plants*, 2(4), pp. 1-6.
- Chen, C. C., Lu, C. S., Chung, Y. C. and Jan, J. L., 2006. UV light induced photodegradation of malachite green on TiO₂ nanoparticles. *Journal of Hazardous Materials* 141, pp. 520-528.
- Combaut, G. and Piovetti, L., 1983. A novel acyclic diterpene from the brown alga *bifurcaria bifurcata*. *Phytochemistry*, 22(8), pp. 1787-1789.
- Cuevas, R., Duran, N., Diez, M. C., Tortella, G. R. and Rubilar, O., 2015. Extracellular biosynthesis of copper and copper oxide nanoparticles by *Stereum hirsutum*, a native white-rot fungus from Chilean forest. *Journals of Nanomaterials*, pp. 1-7.

- Culioli, G., Ortalo-Magne, A., Daoudi, M., Thomas-Guyon, H., Valls, R. and Piovetti, L., 2004. Trihydroxylated linear diterpenes from the brown alga *Bifurcaria bifurcata*. *Phytochemistry*, 65(14), pp. 2063-2069.
- Daoudi, M., Bakkas, S., Culioli, G., Ortalo-Magne, A., Piovetti, L. and Guiry, M. D., 2001. Acyclic diterpenes and sterols from the genera *Bifurcaria* and *Bifurcariopsis* (Cystoseiraceae, Phaeophyceae). *Biochemical Systematics and Ecology* 29, pp. 973-978.
- Devi, H. S. and Singh, T. D., 2014. Synthesis of copper oxide nanoparticles by a novel method and its application in the degradation of methyl orange. *Advance in Electronic and Electric Engineering*, 4(1), pp. 83-88.
- Dinesh, K. P., Patel, K. and Dhanabal, S., 2012. Phytochemical standardization of *Aloe vera* extract by HPTLC techniques. *Journal of Acute Disease*, pp. 47-50.
- Du, L., Jiang, H., Liu, X. and Wang, E., 2007. Biosynthesis of gold nanoparticles assisted by *Escherichia coli* DH5 α and its application on direct electrochemistry of haemoglobin. *Electrochemistry Communications*, 9(5), pp. 1165-1170.
- El-Sayed, G. O., Dessouki, H. A., Jahin, H. S. and Ibrahiem, S. S., 2014. Photocatalytic degradation of Metronidazole in aqueous solutions by copper oxide nanoparticles. *Journal of Basic and Environmental Sciences 1*, pp. 102-110.
- Etefagh, R., Azhir, E. and Shahtahmasebi, N., 2013. Synthesis of CuO nanoparticles and fabrication of nanostructural layer biosensors for detecting *Aspergillus niger* fungi. *Science Iranica*, 20(3), pp. 1055-1058.
- Fayaz, A. M., Balaji, K., Girilal, M., Yadav, R., Kalaichelvan, P. T. and Venketesan, R., 2010. Biogenic synthesis of silver nanoparticles and their synergistic effect with antibiotics: A study against gram-positive and gram-negative bacteria. *Nanomedicine: Nanotechnology, Biology, and Medicine*, 6(1), pp. 103-109.
- Ganapuram, B. R., Alle, M., Dadigala, R., Dasari, A., Maragoni, V. and Guttena, V., 2015. Catalytic reduction of methylene blue and congo red dyes using green synthesized gold nanoparticles capped by salmalia malabarica gum. *International Nano Letters* 5, pp. 215-222.

- Gardea, J. L., Gomez, E., Jose-Yacaman, M., Parson, J. G., Peralta-Videa, J. R. and Tioani, H., 2003. Alfafa sprouts: a natural source for the synthesis of silver nanoparticles. *Langmuir*, vol 19, pp. 1357-1361.
- Ghorbani, H. R., 2014. Chemical synthesis of Copper nanoparticles. *Oriental Journal of Chemistry*, 30(2), pp. 803-806.
- Ghorbani, H. R., Fazeli, I. and Fallahi, A. A., 2015. Biosynthesis of copper oxide nanoparticles using extract of E.coli. *Oriental Journal of Chemistry*, 31(1), pp. 515-517.
- Gopalkrishnan, K., Ramesh, C., Raghunathan, V. and Thamilselvan, M., 2012. Antibacterial activity of Cu₂O nanoparticles on *E. coli* synthesized from *Tridax procumbens* leaf extract and surface coating with polyaniline. *Digest Journal of Nanomaterials and Biostructures*, 7(2), pp. 833-839.
- Guo, H., Ke, Y., Wang, D., Lin, K., Shen, R., Chen, J. and Weng, W., 2013. Efficient adsorption and photocatalytic degradation of Congo red onto hydrothermally synthesized NiS nanoparticles. *Journal of Nanoparticles Research*, 15(3), pp. 1475-1487.
- Herrera-Becerra, R., Zorrilla, C., Rius, J. L. and Ascencio, A., 2008. Electron microscopy characterization of biosynthesized iron oxide nanoparticles. *Applied Physics A*, 91(2), pp. 241-246.
- Honary, S., Barabadi, H., Gharaei-Fathabad, E. and Naghibi, F., 2012. Green synthesis of copper oxide nanoparticles using *Penicillium aurantiogriseum*, *Penicillium citrinum* and *Penicillium waksmaii*. *Digest Journal of Nanomaterials and Biostructures*, 7(3), pp. 999-1005.
- Ibrahim, H. M. M., 2015. Green synthesis and characterization of silver nanoparticles using banana peel extract and their antimicrobial activity against representative microorganisms. *Journal of Radiation Research and Applied Sciences*, 8(3), pp. 265-275.
- Jain, D., Daima, H. K., Kachhwaha, S., Kothari, S. L., 2009. Synthesis of plant-mediated silver nanoparticles using papaya fruit extract and evaluation of their anti-microbial activities. *Digest Journal of Nanomaterials and Biostructures*, 4(4), pp. 723-727.

- Jayalakshmi and Yogamoorthi, A., 2014. Green synthesis of copper oxide nanoparticles using aqueous extract of flowers of *Cassia alata* and particles characterization. *Internal Journal of Nanomaterials and Biostructures*, 4(4), pp. 66-71.
- Joshua, P. J., Krishnan, S., Vidhya Raj, D. J., Uthrakumar, R., Laxmi, S. and Jerome Das, S., 2014. Novel synthesis of tenorite (CuO) nanoparticles by wet chemical method. *International Journal of ChemTech Research*, 6(3), pp. 2002-2004.
- Kalishwaralal, K., Deepak, V., Ram Kumar Pandian, S., Kottaisamy, M., BarathManiKanth, S., Kartikeyan, B. and Gurunathan, S., 2010. Biosynthesis of silver and gold nanoparticles using *Brevibacterium casei*. *Colloids and Surfaces B*, 77(2), pp. 257-262.
- Kanazawa, K. and Sakakibara, H., 2000. High content of dopamine, a strong antioxidant, in Cavendish banana. *Journal of Agricultural and Food Chemistry*, 48(3), pp. 844-848.
- Katwal, R., Kaur, H., Sharma, G., Naushad, M. and Pathania, D., 2015. Electrochemical synthesized copper oxide nanoparticles for enhanced photocatalytic and antimicrobial activity. *Journal of Industrial and Engineering Chemistry* 31, pp. 173-184.
- Katwal, R., Kaur, H., Sharma, G., Naushad, M. and Pathania, D., 2015. Electrochemical synthesis copper oxide nanoparticles for enhanced photocatalytic and antimicrobial activity. *Journal of Industrial and Engineering Chemistry*, vol 31, pp. 173-184.
- Kessler, R., 2011. Engineered Nanoparticles in Consumer Products: Understanding a New Ingredient. *Environmental Health Perspectives*, 119(3), pp. 120-125.
- Khalil, M. H., Ismail, E. H., El-Baghdady, K. Z. and Mohamed, D., 2014. Green synthesis of silver nanoparticles using olive leaf extract and its antibacterial activity. *Arabian Journal of Chemistry*, 7(6), pp. 1131-1139.
- Kitching, M., Ramani, M. and Marsili, E., 2015. Fungi biosynthesis of gold nanoparticles: mechanism and scale up. *Microbial biotechnology*, 8(6), pp. 904-917.

- Kitowaki, H., Oku, T., Akimaya, T. and Suzuki, A., 2012. Fabrication and characterization of CuO-based solar cells. *Journal of Materials Science Research*, 1(1), pp. 138-143.
- Konishi, Y., Ohno, K., Saitoh N., Nomura, T., Nagamine, S., Hishida, H., Takashi, Y. and Uruga, T., 2007. Bioreductive deposition of platinum nanoparticles on the bacterium *Shewanella algae*. *Journal of Biotechnology*, 128(3), pp. 648-653.
- Konishi, Y., Tsukiyama, T., Tachimi, T., Saitoh, N., Nomura, T. and Nagamine, S., 2007. Microbial deposition of gold nanoparticles by the metal-reducing bacterium *Shewanella algae*. *Electrochimica Acta*, 53(1), pp. 186-192.
- Kooti, M. and Matouri, L., 2010. Fabrication of nanosized cuprous oxide using Fehling's solution. *Transaction F: Nanotechnology*, 17(1), pp. 73-78.
- Kumar, P. P. N. V., Shammem, U., Kollu, P., Kalyani, R. L. and Pammin, S. V. N., 2015. *BioNanoScience*, 5(2), pp. 65-122.
- Kumawat, P., Joshi, M., Ameta, J. R. and Ameta, S. C., 2015. Synthesis and use of quaternary oxide $\text{FeZn}_2\text{Cu}_3\text{O}_{6.5}$ as a photocatalyst. *Indian Journal of Science Research and Technology*, 3(4), pp. 72-77.
- Lee, H. J., Lee, G., Jang, N. R., Yun, J. H., Song, J. Y. and Kim, B. S., 2011. Biological synthesis of copper nanoparticles using plant extract. *Nanotechnology*, vol 1, pp. 371-374.
- Lee, J. H., Han, J., Choi, H. and Hur, H. G., 2007. Effects of temperature and dissolved oxygen on Se(IV) removal and Se(0) precipitation by *Shewanella* sp. HN-41. *Chemosphere*, 68(10), pp. 1898-1905.
- Li, Y., 2008. Synthesis of copper(II) oxide particle and detection of photoelectrochemically generated hydrogen. *NNIN REU Research Accomplishments*, pp. 46-47.
- Lloyd, J. R., Yong, P. and Macaskie, L. E., 1998. Enzymatic recovery of elemental palladium by using sulphate-reducing bacteria. *Applied and Environmental Microbiology*, 64(11), pp. 4607-4609.
- Luna, I. Z., Hilary, L. N., Chowdhury, A. M. S., Gafur, M. A., Khan, N. and Khan, R. A., 2015. Preparation and characterization of copper oxide nanoparticles synthesized via chemical precipitation method. *Open Access Library Journal*, vol 2, e1409.

- Makarov, V. V., Love, A. J., Sinitsyna, O. V., Makarova, S. S., Yaminsky, I. V., Taliansky, M. E. and Kalinina, N. O., 2014. "Green" nanotechnologies: synthesis of metal nanoparticles using plants. *Acta Naturae*, 6(1), pp. 35-44.
- Manimaran, R., Palaniradja, K., Alagumurthi, N., Sendhilnathan, S. and Hussain, J., 2013. Preparation and characterization of copper oxide nanofluid for heat transfer applications. *Applied Nanoscience*, 4(2), pp. 163-167.
- Mathew, B. B., Jatawa, S. K. and Tiwari, A., 2012. Phytochemical analysis of *Citrus limonum* pulp and peel. *International Journal of Pharmacy and Pharmaceutical Sciences*, 4(2), pp. 269-371.
- Mohan, S., Singh, Y., Verma, D. K. and Hasan, S. H., 2015. Synthesis of CuO nanoparticles through green route using *Citrus limon* juice and its application as nanosorbent for Cr(IV) remediation: Process optimization with RSM and ANN-GA based model. *Process Safety and Environmental Protection*, pp. 156-166.
- Movahedi, M., Mahjoub, A. R. and Janitabar-Darzi, S., 2009. Photodegradation of Congo Red in aqueous solution on ZnO as an alternative catalyst to TiO₂. *Journal of the Iranian Chemical Society*, 6(3), pp. 570-577.
- Mude, N., Ingle, A., Gade, A. and Rai, M., 2009. Synthesis of silver nanoparticles by the callus extract of *Carica papaya*: a first report. *Journal of Biochemistry and Biotechnology*, vol 18, pp. 83-86.
- Munoz, J., Culioli, G., Kock, M., 2012. Linear diterpenes from the marine brown algae *Bifurcaria bifurcata*: a chemical perspective. *Phytochemistry Reviews*, 12(3), pp. 407-424.
- Naika, H. R., Lingaraju, K., Manjunath, K., Kumar, D., Nagaraju, G., Suresh, D. and Nagabhushana, H., 2015. Green synthesis of CuO nanoparticles using *Gloriosa superba* L. extract and their antibacterial activity. *Journal of Taibah University for Science* 9, vol 2015, pp. 7-12.
- Oikeh, E. I., Omoregie, E. S., Oviasogie, F. E. and Oriakhi, K., 2016. Phytochemical, antimicrobial, and antioxidant activities of different citrus juice concentrates. *Food Science & Nutrition*, 4(1), pp. 103-109.

- Outokesh, M., Hosseinpour, M., Ahmadi, S. J., Mousavand, T., Sadjadi, S. and Soltanian, W., 2011. Hydrothermal synthesis of CuO nanoparticles: study on effects of operational conditions on yield, purity, and size of the nanoparticles. *Industrial & Engineering Chemistry Research*, vol 50, pp. 3540-3554.
- Phiwdang, K., Suphankij, S., Mekprasart, W. and Pecharapa, W., 2013. Synthesis of CuO nanoparticles by precipitation method using different precursors. *Energy Procedia*, vol 34, pp. 740-745.
- Prasad, R., 2014. Synthesis of Silver Nanoparticles in Photosynthetic Plants. *Journal of Nanoparticles*, vol 2014, pp. 1-8.
- Qu, J., Yuan, X., Wang, X. and Shao, P., 2011. Zinc accumulation and synthesis of ZnO nanoparticles using *Physalid alkekengi* L. *Environmental Pollution*, 159(7), pp. 1783-1788.
- Rahman, A., Ismail, A., Jumbianti, D., Magdalena, S. and Sudrajat, H., 2009. Synthesis of copper oxide nanoparticles by using *Phoridium cyanibacterium*. *Indonesian Journal of Chemistry*, 9(3), pp. 355-360.
- Rao, A. N. S. and Venkatarangaiah, V. T., 2014. The effect of cetyltrimethylammonium bromide on size and morphology of ZnO and CuO. *Journal of Electrochemical Science and Engineering*, 4(3), pp. 97-110.
- Raphael, E., 2012. Phytochemical constituents of some leaves extract of Aloe vera and Azadirachta indica plant species. *Global Advanced Research Journal of Environmental Science and Toxicology*, 1(2), pp. 14-17.
- Ren, G., Hu, D., Cheng, W. C., Vargus-Reus, M. A., Reip, P. and Allaker, R. P., 2009. Characterization of copper oxide nanoparticles for antimicrobial applications. *International Journal of Antimicrobial Agents*, 33(6), pp. 587-590.
- Roco, M. C., 2011. The long view of nanotechnology development: the National Nanotechnology Initiative at 10 years. *Nanotechnology Research Directions for Societal Needs in 2020*, vol 13, pp. 427-445.
- Roy, T. K. and Mondal, N. K., 2014. Photocatalytic degradation of Congo red dye on thermally activated zinc oxide. *International Journal of Scientific Research in Environmental Sciences*, 2(12), pp. 457-469.

- Saikia, L., Bhuyan, D., Saikia, M., Malakar, B., Dutta, D. K. and Sengupta, P., 2015. Photocatalytic performance of ZnO nanomaterials for self sensitized degradation of malachite green dye under solar light. *Applied Catalyst A: General* 490, pp. 42-49.
- Sankar, R., Manikandan, P., Malarvizhi, V., Fathima, T. and Shivashangari, K. S. and Ravikumar, V., 2014. Green synthesis of colloidal copper oxide nanoparticles using *Carica papaya* and its application in photocatalytic dye degradation. *Spectrochimica Acta Part A: Molecular and Biomolecular Spectroscopy* 121, pp. 746-750.
- Seabra, A. and Duran, K., 2015. Nanotoxicology of Metal Oxide Nanoparticles. *Metals*, vol 5, pp. 934-975.
- Sema, E., Aksu, S. K., Saylkan, F., Izgi, B., Asilturk, M., Saylkan, H., Frimmel, F. and Gucer, S., 2008. Photocatalytic degradation of Congo Red by hydrothermally synthesized nanocrystalline TiO₂ and identification of degradation products by LC-MS. *Journal of Hazardous Materials* 155, pp. 469-476.
- Sen, J., Prakash, P. and De, N., 2015. Nano-clay composite and phyto-nanotechnology: a new horizon to food security issue in Indian agriculture. *Journal of Global Biosciences*, 4(5), pp. 2187-2198.
- Shankar, S. S., Ahmad, A., Pasricha, R. and Sastry, M., 2003. Bioreduction of chloroaurate ions by *Geranium* leaves and its endophytic fungus yields gold nanoparticles of different shapes. *Journal of Materials Chemistry*, vol 13, pp. 1822-1826.
- Sharma, P. and Sharma, S. K., 2012. Photocatalytic degradation of cuprous oxide nanostructures under UV/Visible irradiation. *Water Resources Management*, 30(242).
- Sheny, D. S., Philip, D. and Mathew, J., 2012. Rapid green synthesis of palladium nanoparticles using the dried leaf of *Anacardium occidentale*. *Spectrochim Acta Part A: Molecular and Biomolecular Spectroscopy*, 91, pp. 35-38.
- Singaravelu, G., Arockiamary, J. S., Kumar, V. G. and Govindaraju, K., 2007. A novel extracellular synthesis of monodisperse gold nanoparticles using marine alga, *Sargassum wightii* Greville. *Colloids and Surfaces B*, 57(1), pp. 97-101.

- Sinha, A. and Khare, S. K., 2011. Mercury bioaccumulation and simultaneous nanoparticle synthesis by *Enterbacter sp.* Cells. *Bioresource Technology*, vol 102, pp. 4281-4284.
- Singh, P., Kim, Y., Zhang, D. and Yang, D., 2016. Biological Synthesis of Nanoparticles from Plants and Microorganisms. *Trends in Biotechnology*, 34(7), pp. 588-599.
- Someya, S., Yoshiki, Y. and Okubo, K., 2002. Antioxidant compounds from bananas (*Musa Cavendish*). *Food Chemistry*, 79(3), pp. 351-354.
- Suleiman, M., Mousa, M., Hussein, A., Hammouti, B., Hadda, T. B. and Warad, I., 2013. Copper(II)-oxide nanostructures: synthesis, characterization and their applications-reviews. *Journal of Materials and Environmental Science*, 4(5), pp. 792-797.
- Sundaram, S., Anjum, S., Dwivedi, P. and Rai, G. K., 2011. Antioxidant activity and protective effect of banana peel against oxidative hemolysis of human erythrocyte at different stages of ripening. *Applied Biochemistry and Biotechnology*, 164(7), pp. 1192-1206.
- Sundaramurthy, N. and Parthiban, C., 2015. Biosynthesis of copper oxide nanoparticles using *Pryus Pyrifolia* leaf extract and evolve the catalytic activity. *International Research Journal of Engineering and Technology*, 2(6), pp. 332-338.
- Tenkyong, T., Neena Bachan, J., Raja, P., Naveen Kumar, J. and Shyla, M., 2015. Investigation of sol-gel processed CuO/SiO₂ nanocomposite as a potential photoanode materials. *Materials Science-Poland*, 33(4), pp. 826-834.
- Thi, T. V., Rai, A. K., Gim, J. and Kim, J., 2014. Potassium-doped copper oxide nanoparticles synthesized by solvothermal method as an anode material for high-performance lithium ion secondary battery. *Applied Surface Science*, vol 305, pp. 617-625.
- Tiwari, D.K., Behari, J. and Sen, P., 2008. Application of nanoparticles in waste water treatment. *World Applied Sciences Journal*, 3(3), pp. 417-433.
- Valls, R., Banaigs, B., Piovetti, L., Archavlis, A., Artaud, J., 1993. Linear diterpenes with antimitotic activity from the brown alga *Bifurcaria bifurcata*. *Phytochemistry*, 34(6), pp. 1585-1588.

- Wu, R., Ma, Z., Gu, Z. and Yang, Y., 2010. Preparation and characterization of CuO nanoparticles with different morphology through a simple quick-precipitation method in DMAC–water mixed solvent. *Journal of Alloys and Compounds* 504, pp. 45-49.
- Yao, W. T., Yu, S. H., Zhou, Y., Jiang, Y., Wu, Q. S., Zhang, L. and Jiang, J., 2005. Formation of uniform CuO nanorods by spontaneous aggregation: selective synthesis of CuO, Cu₂O and Cu nanoparticles by a solid-liquid phase arc discharge process. *Journal of Physical Chemistry B*, 109(29), pp. 14011-14016.
- Zhang, L., Yuan, F., Zhang, X and Yang, L. 2011. Facile synthesis of flower like copper oxide and their application to hydrogen peroxide and nitrite sensing. *Chemistry Central Journal*, 5(75), pp. 220-227.
- Zhou, Y., Lin, W., Huang, J., Wang, W., Gao, Y., Lin, L., Li, Q., Lin, L. and Du, M., 2010. Biosynthesis of Gold Nanoparticles by Foliar Broths: Roles of Biocompounds and Other Attributes of the Extracts. *Nanoscale Research Letters*, 5(8), pp. 1351-1359.
- Zubia, M., Fabre, M. S., Kerjean, V., Lann, K. L., Stiger-Pouvreau, V., Fauchon, M. and Deslandes, E., 2009. *Food Chemistry* 116, pp. 693-701.

e-book

- Kung, H. H., 1989. *Transition metal oxides: surface chemistry and catalysis*. [e-book] Elsevier science publishing company. Available at: Google Books<https://books.google.com.my/books?id=S4Cbzt6_OSYC&pg=PA1&lpg=PA1&dq=metal+oxides+chemistry+introduction&source=bl&ots=QE5SOI9QGu&sig=cm3LZdMHwM8USTTdpwjHgvMl1b4&hl=en&sa=X&redir_esc=y#v=onepage&q=metal%20oxides%20chemistry%20introduction&f=false> [Accessed 16 July 2016]

Edited book

- Ardelean, I. I., 2015. Metallic Nanoparticle Synthesis by Cyanobacteria: Fundamentals and Applications. In: Sahoo, D. and Seckbach, J., ed. 2015 *The Algae World*. New York London: Springer Dordrecht Heidelberg. pp. 437.

Habiba, K., Makarov, V. I., Weiner, B. R. and Morell, G., 2014. Fabrication of Nanomaterials by Pulsed Laser Synthesis. In: Waqar, A and Ali, N. *Manufacturing Nanostructures*. UK: One Central Press (OCN). pp. 263-291.

Magazine articles

Choudhary, V., 2016. Medicinal uses of *Gloriosa superba* (Flame lily). *Abhinav Nature Conservation*, [online] Available at: <<http://natureconservation.in/medicinal-uses-of-gloriosa-superba-flame-lily/>> [Accessed 17 July 2016]

Internet websites

International Iberian Nanotechnology Laboratory, n.d. *Background Information on Nanotechnology*. [online] Available at: <http://www.unic.pt/images/stories/Background_Nanotechnology.pdf> [Accessed 13 July 2016]

Progetti, P., 2016. *List of nanotechnology applications*. [online] Available at: <<http://bionanotech.uniss.it/?p=760>> [Accessed 14 July 2016]

APPENDICES

Appendix A

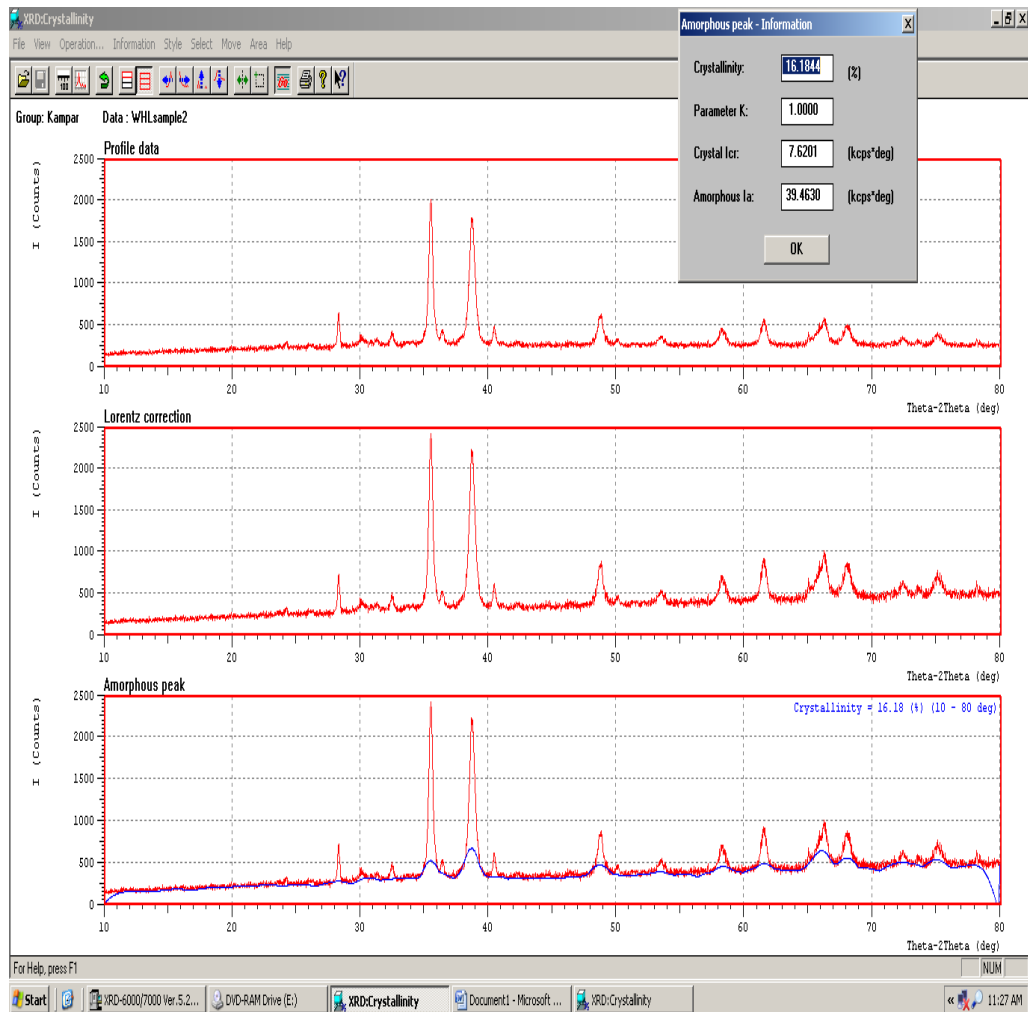


Figure: Information of crystallinity of CuO NPs.

Appendix B

Calculation of Crystalline Size using Debye-Scherrer Equation

To calculate β

$$\begin{aligned}\beta &= \frac{(\text{FWHM in } 2\theta \times \pi)}{180^\circ} \\ &= \frac{(0.36880 \times \pi)}{180^\circ} \\ &= 6.4368 \times 10^{-3}\end{aligned}$$

Debye-Scherrer Equation

$$\begin{aligned}D &= \frac{k \lambda}{(\beta \cos \theta)} \\ &= \frac{(0.9 \times 1.5406 \times 10^{-10} \text{ m})}{(6.4368 \times 10^{-3} \cos 17.7623^\circ)} \\ &= \frac{1.38654 \times 10^{-10}}{(6.1300 \times 10^{-3})} \\ &= 2.26 \times 10^{-8} \text{ m} \\ &= 22.60 \text{ nm}\end{aligned}$$

where

β = width of a diffraction peak at full-width half maximum

FWHM = full-width half maximum

D = crystalline size in diameter

k = shape factor (usually is 0.9)

λ = wavelength of X-ray source (Cu K_α radiation = $1.5406 \times 10^{-10}\text{m}$)

θ = diffraction angle

Appendix C

$$\text{Degradation percentage} = \frac{(A_0 - A_t)}{A_0} \times 100 \%$$

where

A_0 = initial absorbance of dye solution

A_t = absorbance of dye solution at different time intervals

Effects of Contact Time in Degradation of Congo Red by CuO NPs

Contact time (min)	Initial absorbance	Final absorbance	Degradation percentage (%)
0	0.394	0.394	0
15	0.394	0.208	47.21
30	0.394	0.193	51.02
45	0.394	0.138	64.97
60	0.394	0.122	69.04
90	0.394	0.091	76.90
120	0.394	0.057	85.53
150	0.394	0.044	88.83

Table: Degradation percentage of Congo red as a function of contact time.

Appendix D

Contact time (min)	Initial absorbance	Final absorbance	Degradation percentage (%)
0	1.533	1.533	0
10	1.533	0.425	72.28
20	1.533	0.298	80.56
30	1.533	0.284	81.47
60	1.533	0.268	82.52
90	1.533	0.249	83.76
120	1.533	0.211	86.24
180	1.533	0.183	88.06
240	1.533	0.126	91.78

Table: Degradation percentage of Malachite green as a function of contact time.

Appendix E

*** Basic Data Process ***

Group : Kampar
Data : WHLsample2

Strongest 3 peaks

no.	peak no.	2Theta (deg)	d (Å)	I/I1	FWHM (deg)	Intensity (Counts)	Integrated Int (Counts)
1	7	35.5246	2.52500	100	0.36880	1157	23511
2	9	38.7523	2.32180	87	0.49090	1012	29843
3	11	48.7628	1.86600	22	0.47430	249	6544

Peak Data List

peak no.	2Theta (deg)	d (Å)	I/I1	FWHM (deg)	Intensity (Counts)	Integrated Int (Counts)
1	24.2234	3.67127	3	0.23890	38	694
2	28.3238	3.14842	19	0.24900	218	2883
3	30.1133	2.96527	6	0.37330	65	1713
4	31.2946	2.85598	4	0.35930	43	1042
5	32.4966	2.75303	8	0.30890	94	1623
6	34.9400	2.56590	4	0.20000	43	1238
7	35.5246	2.52500	100	0.36880	1157	23511
8	36.4113	2.46552	9	0.29120	102	1994
9	38.7523	2.32180	87	0.49090	1012	29843
10	40.4846	2.22636	11	0.27330	132	2186
11	48.7628	1.86600	22	0.47430	249	6544
12	49.3000	1.84691	3	0.22000	39	770
13	50.0975	1.81937	4	0.29500	48	828
14	53.4800	1.71200	6	0.52000	69	1785
15	53.7800	1.70315	3	0.31200	37	553
16	58.2900	1.58166	11	0.58000	133	4344
17	61.5218	1.50609	17	0.48360	199	5555
18	65.0739	1.43220	6	0.26350	73	930
19	65.6800	1.42044	8	0.55200	94	2644
20	65.9400	1.41547	12	0.00000	135	0
21	66.3000	1.40866	19	0.33000	216	5307
22	68.0187	1.37719	13	0.60250	154	5663
23	72.3941	1.30435	5	0.47830	56	1797
24	73.5800	1.28623	3	0.26000	37	642
25	75.0600	1.26449	8	0.52000	87	2176
26	75.4400	1.25907	4	0.33600	51	1062
27	78.2150	1.22119	4	0.22340	46	724

Figure: XRD information of synthesized nanoparticles (Part I).

Appendix F

```
*** Basic Data Process ***

# Data Infomation
  Group           : Kampar
  Data            : WHLsample2
  Sample Nmae    : WHLsample2
  Comment         :
  Date & Time     : 06-24-16 10:12:56

# Measurement Condition
  X-ray tube
    target        : Cu
    voltage       : 40.0 (kV)
    current       : 30.0 (mA)
  Slits
    Auto Slit     : not Used
    divergence slit : 1.00000 (deg)
    scatter slit  : 1.00000 (deg)
    receiving slit : 0.30000 (mm)
  Scanning
    drive axis    : Theta-2Theta
    scan range    : 10.0000 - 80.0000 (deg)
    scan mode     : Continuous Scan
    scan speed    : 2.0000 (deg/min)
    sampling pitch : 0.0200 (deg)
    preset time   : 0.60 (sec)

# Data Process Condition
  Smoothing       [ AUTO ]
    smoothing points : 21
  B.G.Subtruction [ AUTO ]
    sampling points  : 21
    repeat times     : 30
  Kal-a2 Separate [ MANUAL ]
    Kal a2 ratio     : 50 (%)
  Peak Search     [ AUTO ]
    differential points : 19
    FWHM threshold    : 0.050 (deg)
    intensity threshold : 30 (par mil)
    FWHM ratio (n-1)/n : 2
  System error Correction [ NO ]
  Precise peak Correction [ NO ]
```

Figure: XRD information of synthesized nanoparticles (Part II).

Appendix G

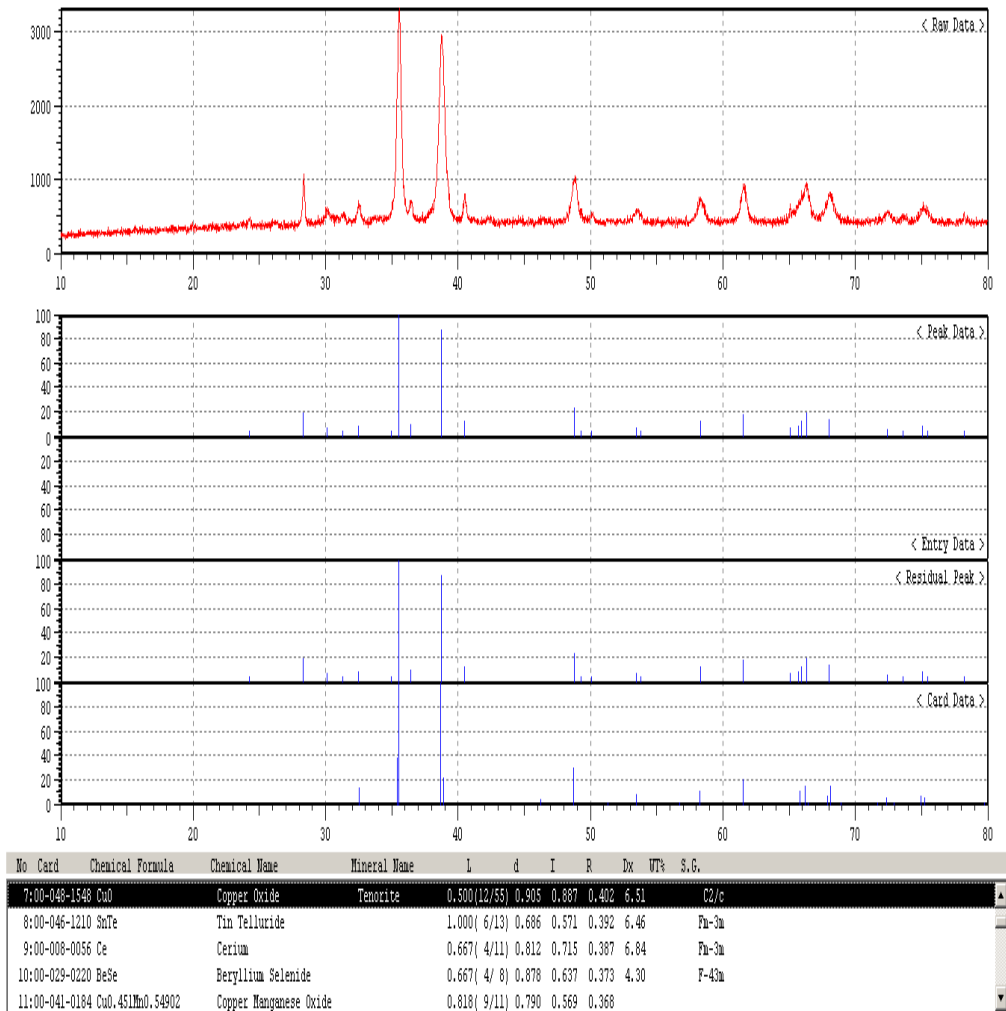


Figure: Synthesized CuO NPs, JCPDS 048-1548.